

1 **A large sample analysis of European rivers on seasonal river flow correlation**
2 **and its physical drivers**

3 Theano Iliopoulou^{1*}, Cristina Aguilar², Berit Arheimer³, María Bermúdez⁴, Nejc Bezak⁵, Andrea
4 Ficchi⁶, Demetris Koutsoyiannis¹, Juraj Parajka⁷, María José Polo², Guillaume Thirel⁸ and
5 Alberto Montanari⁹

6 ⁽¹⁾ Department of Water Resources and Environmental Engineering, School of Civil Engineering,
7 National Technical University of Athens, Zographou, 15780, Greece

8 ⁽²⁾ Fluvial dynamics and hydrology research group, Andalusian Institute of Earth System
9 Research, University of Cordoba, Cordoba, 14071, Spain

10 ⁽³⁾ Swedish Meteorological and Hydrological Institute, 601 76 Norrköping, Sweden

11 ⁽⁴⁾ Water and Environmental Engineering Group, Department of Civil Engineering, Universidade
12 da Coruña, 15071 A Coruña, , Spain

13 ⁽⁵⁾ Faculty of Civil and Geodetic Engineering, University of Ljubljana, Jamova 2, SI-1000
14 Ljubljana, Slovenia

15 ⁽⁶⁾ Department of Geography and Environmental Science, University of Reading, Reading, RG6
16 6AB, United Kingdom; formerly, IRSTEA, Hydrology Research Group (HYCAR), F-92761,
17 Antony, France

18 ⁽⁷⁾ Vienna University of Technology, Institute of Hydraulic Engineering and Water Resources
19 Management, Karlsplatz 13/222, A-1040 Vienna, Austria

20 ⁽⁸⁾ IRSTEA, Hydrology Research Group (HYCAR), F-92761, Antony, France

21 ⁽⁹⁾ Department DICAM, University of Bologna, Bologna, 40136, Italy

22 * *Correspondence to:* Theano Iliopoulou (anyily@central.ntua.gr)

23
24
25
26

27 **Abstract**

28 The geophysical and hydrological processes governing river flow formation exhibit persistence
29 at several timescales, which may manifest itself with the presence of positive seasonal
30 correlation of streamflow at several different time lags. We investigate here how persistence
31 propagates along subsequent seasons and affects low and high flows. We define the High Flow
32 Season (HFS) and the Low Flow Season (LFS) as the three-month and the one-month periods
33 which usually exhibit the higher and lower river flows, respectively. A dataset of 224 rivers from
34 six European countries spanning more than 50 years of daily flow data is exploited. We compute
35 the lagged seasonal correlation between selected river flow signatures, in HFS and LFS, and the
36 average river flow in the antecedent months. Signatures are peak and average river flow for HFS
37 and LFS, respectively. We investigate the links between seasonal streamflow correlation and
38 various physiographic catchment characteristics and hydro-climatic properties. We find
39 persistence to be more intense for LFS signatures than HFS. To exploit the seasonal correlation
40 in the frequency estimation of high and low flows, we fit a bivariate Meta-Gaussian probability
41 distribution to the selected flow signatures and average flow in the antecedent months in order to
42 condition the distribution of high and low flows in the HFS and LFS, respectively, upon river
43 flow observations in the previous months. The benefit of the suggested methodology is
44 demonstrated by updating the frequency distribution of high and low flows one season in
45 advance in a real-world case. Our findings suggest that there is a traceable physical basis for
46 river memory which in turn can be statistically assimilated into high- and low-flow frequency
47 estimation to reduce uncertainty and improve predictions for technical purposes.

48

49 **Keywords:** seasonal streamflow correlation, river memory, persistence, real-time flow
50 forecasting, floods, low flows, meta-Gaussian

51 **1. Introduction**

52 Recent analyses for the Po River and the Danube River highlighted that catchments may exhibit significant
53 correlation between peak river flows and average flows in the previous months (Aguilar et al., 2017). Such
54 correlation is the result of the behaviours of the physical processes involved in the rainfall-runoff
55 transformation that may induce memory in river flows at several different time scales. The presence of
56 long-term persistence in streamflow has been known for a long time since the pioneering works of Hurst
57 (1951) and has been actively studied ever since (e.g. Koutsoyiannis, 2011; Montanari, 2012; O’Connell et
58 al., 2016 and references therein). While a number of seasonal flow forecasting methods have been explored
59 in the literature (e.g. Bierkens and van Beek, 2009; Dijk et al., 2013), attempts to explicitly exploit
60 streamflow persistence in seasonal forecasting through information from past flows have been in general
61 limited. Koutsoyiannis et al. (2008) proposed a stochastic approach to incorporate persistence of past flows
62 into a prediction methodology for monthly average streamflow and found the method to outperform the
63 historical analogue method (see also Dimitriadis et al., 2016 for theory and applications of the latter) and
64 artificial neural network methods in the case of the Nile River. Similarly, Svensson (2016) assumed that the
65 standardized anomaly of the most recent month will not change during future months to derive monthly
66 flow forecasts for 1–3 months lead time and found the predictive skill to be superior to the analogue
67 approach for 93 UK catchments. The abovementioned persistence approach has also been used
68 operationally in the production of seasonal streamflow forecasts in the UK since 2013, within the
69 framework of the Hydrological Outlook UK (Prudhomme et al. 2017). A few other studies have included
70 past flow information in prediction schemes along with teleconnections or other climatic indices (Piechota
71 et al., 2001; Chiew et al., 2003; Wang et al., 2009). Recently, it was shown that streamflow persistence,
72 revealed as seasonal correlation, may also be relevant for prediction of extreme events by allowing one to
73 update the flood frequency distribution based on river flow observations in the pre-flood season and reduce
74 its bias and variability (Aguilar et al., 2017). The above previous studies postulated that seasonal

75 streamflow correlation may be due to the persistence of the catchments storage and/or the weather, but no
76 attempt was made to identify the physical drivers.

77 The present study aims to further inspect seasonal persistence in river flows and its determinants, by
78 referring to a large sample of catchments in 6 European countries (Austria, Sweden, Slovenia, France,
79 Spain and Italy). We focus on persistence properties of both high and low flows by investigating the
80 following research questions: (i) what are the physical conditions, in terms of catchment properties, i.e.
81 geology and climate, which may induce seasonal persistence in river flow? And, (ii) can floods and
82 droughts be predicted, in probabilistic terms, by exploiting the information provided by average flows in
83 the previous months? These questions are relevant for gaining a better comprehension of catchment
84 dynamics and planning mitigation strategies for natural hazards. To reach the above goals, we identify a set
85 of descriptors for catchment behaviours and climate, and inspect their impact on correlation magnitude and
86 predictability of river flows.

87 A few studies have analysed physical drivers of streamflow persistence on annual and deseasonalized
88 monthly and daily timeseries (Mudelsee, 2007; Hirpa et al., 2010; Gudmundsson et al., 2011; Zhang et al.,
89 2012; Szolgayova et al., 2014; Markonis et al., 2018) but the topic has been less studied on intra-annual
90 scales relevant to seasonal forecasting of floods and droughts.

91 To demonstrate the high practical relevance of the identified seasonal correlations we present a
92 technical experiment for one of the studied rivers (Section 7) in which the frequency distribution of both
93 high and low flows is updated one season in advance by exploiting real-time information on the state of the
94 catchment.

95 **2. Methodology**

96 The investigation of the persistence properties of river flows focuses separately on both high and low
97 discharges and is articulated in the following steps: (a) identification of the high- and low-flow seasons; (b)
98 correlation assessment between the peak flow in the high flow season (average flow in the low-flow
99 season) and average flows in the previous months; (c) analysis of the physical drivers for streamflow

100 persistence and its predictability through a Principal Component Analysis; (d) real-time updating of the
101 frequency distribution of high and low flows for a selected case study with significant seasonal correlation
102 by employing a Meta-Gaussian approach. The above steps are described in detail in the following sections.

103 **2.1 Season Identification**

104 Season identification is performed algorithmically to identify the High Flow Season (HFS) and Low Flow
105 Season (LFS) for each river time series. For the estimation of HFS, we employ an automated method
106 recently proposed by Lee et al. (2015), which identifies the high flow season as the three-month period
107 centred around the month with the maximum number of occurrences of Peaks Over Threshold (POT), with
108 the threshold set to the highest 5% of the daily flows. To evaluate the selection of HFS, a metric
109 constructed as the Percentage of Annual Maximum Flows (PAMF) captured in the HFS is used. The
110 PAMFs are classified in subjective categories of “poor” (<40%), “low” (40–60%), “medium” (60–80%)
111 and “high” (>80%) values, denoting the probability that the identified HFS is the dominant high-flow
112 season in the record. If the identified peak month alone contains 80% or more of annual maxima flows, a
113 uni-modal regime is assumed and the identification procedure is terminated. In all other cases, the method
114 allows for the search of a second peak month and the identification of a minor HFS but we do not further
115 elaborate on this analysis here because we are only interested in the most extreme seasons for the purpose
116 of predicting high and low flows.

117 The method proposed by Lee et al. (2015) has several advantages that make it suitable for the purpose
118 of this research. Most importantly, it is capable of handling conditions of bi-modality, which is usually a
119 major issue for traditional methods like, e.g., directional statistics (Cunderlik et al., 2004). A potential
120 limitation is the assumption of symmetrical extension of HFS around the peak month, along with the
121 uniform selection of its length (3-month period). The degree of subjectivity in the evaluation of the second
122 HFS is another limitation, which is not relevant here as we focus on the main HFS.

123 LFS is herein identified as the one-month period with the lowest amount of mean monthly flow. An
124 alternative approach of estimating the relative frequencies of annual minima of monthly flow and selecting
125 the month with the highest frequency as LFS is also considered.

126 **2.2 Correlation analysis and physical interpretation through Principal Component Analysis**

127 *2.2.1 Correlation analysis*

128 In the case of HFS, a correlation is sought between the maximum daily flow occurring in the HFS period
129 and the mean flow in the previous months, before the onset of HFS. For LFS, correlation is computed
130 between the mean flow in the LFS itself and the mean flow in the previous months. We use the mean flow
131 in the previous month as a robust proxy of ‘storage’ in the catchment that is expected to reflect the state of
132 the catchment, i.e., wetter/drier than usual. Since we are interested in seasonal persistence, we compute the
133 Pearson’s correlation coefficient up to 9-month lag for HFS and 11-month lag for LFS.

134 *2.2.2 Analysis of physical drivers*

135 *a. Catchment, geological and climatic descriptors*

136 An extensive investigation is carried out to identify physical drivers of seasonal streamflow correlation, in
137 terms of catchment, geological and climatic descriptors.

138 As catchment descriptors, we consider the basin area (A), the Baseflow Index (BI), the mean specific
139 runoff (SR), the percentage of basin area covered by lakes (percentage of lakes, PL) and glaciers
140 (percentage of glaciers, PG) and altitude as candidate explanatory variables for streamflow correlation.

141 The area A (km^2) is primarily investigated as it is representative of the scale of the catchment, under
142 the assumption that in larger basins the impact of the climatological and geophysical processes affecting
143 river flow becomes more significant and may lead to a magnified seasonal correlation.

144 BI is considered based on the assumption that high groundwater storage may be a potential driver of
145 correlation. BI is calculated from the daily flow series of the rivers following the hydrograph separation
146 procedure detailed in Gustard et al. (2009). Flow minima are sampled from non-overlapping 5-day blocks
147 of the daily flow series and turning points in the sequence of minima are sought and identified when the

148 90% value of a certain minimum is smaller or equal to its adjacent values. Subsequently, linear
149 interpolation is used in between the turning points to obtain the baseflow hydrograph. The BI is obtained as
150 the ratio of the volume of water beneath the baseflow separation curve versus the total volume of water
151 from the observed hydrograph, and an average value is computed over all the observed hydrographs for a
152 given catchment. A low index is indicative of an impermeable catchment with rapid response, whereas a
153 high value suggests high storage capacity and a stable flow regime.

154 SR ($m^3 s^{-1} km^{-2}$) is computed as the mean daily flow of the river standardized by the size of its basin
155 area. It may be an important physical driver as it is an indicator of the catchment's wetness. PL (%) and PG
156 (%) are investigated for the Swedish and Austrian catchments, respectively, as lakes and glaciers are
157 expected to increase catchment storage thus affecting persistence. Lake coverage data are based on
158 cartography and available from the Swedish Water Archive (<https://www.smhi.se/>), while glacier coverage
159 data are estimated from the CORINE land cover database ([https://www.eea.europa.eu/publications/COR0-](https://www.eea.europa.eu/publications/COR0-landcover)
160 [landcover](https://www.eea.europa.eu/publications/COR0-landcover)).

161 The effect of catchment altitude is also inspected using relief maps from the Shuttle Radar
162 Topography Mission (SRTM) data (<http://srtm.csi.cgiar.org/>). The data are available for the whole globe
163 and are sampled at 3 arc-seconds resolution (approximately 90 meters). Topographic information is
164 available for all catchments located at latitude lower than 60 degrees north while a 1 km resolution digital
165 elevation model is available for Austria.

166 As geological descriptors we consider the percentage of catchment area with the presence of flysch
167 (percentage of flysch, PF) and karstic formations (percentage of karst, PK) for Austrian and Slovenian
168 catchments, respectively, for which this type of information is available. A subset of Austrian catchments is
169 characterised by the dominant presence of flysch, a sequence of sedimentary rocks characterized by low
170 permeability, which is known to generate a very fast flow response. Karstic catchments, characterized by
171 the irregular presence of sinkholes and caves, are also known for having rapid response times and complex
172 behaviour; e.g. initiating fast preferential groundwater flow and intermittent discharge via karstic springs

173 (Ravbar, 2013; Cervi et al., 2017). Geological features are presumed to be linked to persistence properties
174 also because geology is the main control for the baseflow index across the European continent (Kuentz et
175 al. 2017). PK (%) and PF (%) are estimated from geological maps of Slovenia and Austria, respectively.

176 As climatic descriptors, the mean annual precipitation P (mm year⁻¹) and the mean annual
177 temperature T (°C) are selected. Corresponding gridded data are retrieved from the Worldclim database
178 (<http://www.worldclim.org/>) at a spatial resolution of 10 minutes of degree (approximately 18.55 km). We
179 note that low mean temperature regimes are also associated with snow, the presence of which is also
180 considered in the interpretation of the results. We also adopt as climatic descriptor the De Martonne index
181 (De Martonne, 1926), IDM, which is given by $IDM = P/(T + 10)$, and enables classification of a region
182 into one of the following 6 climate classes, i.e., arid ($IDM \leq 5$), semi-arid ($5 < IDM \leq 10$), dry sub-humid
183 ($10 < IDM \leq 20$), wet sub-humid ($20 < IDM \leq 30$), humid ($30 < IDM \leq 60$) and very humid ($IDM \geq 60$).
184 Additionally, the Köppen-Geiger climatic classification (Kottek et al., 2006) of the rivers is assessed.

185 *b. Principal Component Analysis*

186 To identify what catchment, physiographic and climatic characteristics may explain river memory we
187 attempt to regress the seasonal streamflow correlation against the physical descriptors introduced above.
188 We expect the presence of multi-collinearity among the explaining variables and therefore Principal
189 Component Analysis (PCA; Pearson, 1901; Hotelling, 1933) was applied to construct uncorrelated
190 explanatory variables. In essence, PCA is an orthonormal linear transformation of p data variables into a
191 new coordinate system of $q \leq p$ uncorrelated variables (principal components, PCs) ordered by decreasing
192 degree of variance retained when the original p variables are projected into them (Jolliffe, 2002). Therefore,
193 the first principal axis contains the greatest degree of variance in the data, while the second principal axis is
194 the direction which maximizes the variance among all directions orthogonal to the first principal axis and
195 so on. Specifically, let \mathbf{x} be a random vector with mean μ and correlation matrix Σ , then the principal
196 component transformation of \mathbf{x} is obtained as follows:

197 $\mathbf{y} = \mathbf{C}^T \mathbf{x}'$ (1)

198 where \mathbf{y} is the transformed vector whose k th column is the k th principal component ($k = 1, 2..p$), \mathbf{C} is the $p \times$
199 p matrix of the coefficients or loadings for each principal component and \mathbf{x}' is the standardized \mathbf{x} vector.
200 Standardization is applied in order to avoid the impact of the different variable units on selecting the
201 direction of maximum variance, when forming the PCs. The \mathbf{y} values are the scores of each observation, i.e.
202 the transformed values of each observation of the original p variables in the k th principal component
203 direction.

204 PCA has useful descriptive properties of the underlying structure of the data. These properties can be
205 efficiently visualized in the biplot (Gabriel, 1971), which is the combined plot of the scores of the data for
206 the first two principal components along with the relative position of the p variables as vectors in the two-
207 dimensional space. Herein, the distance biplot type (Gower and Hand, 1995), which approximates the
208 Euclidean distances between the observations, is used. Variable vectors coordinates are obtained by the
209 coefficients of each variable for the first two principal components. After construction of the PCs, a linear
210 regression model is explored for the case of HFS and LFS lag-1 correlation.

211 **2.3 Technical experiment: Real-time updating of the frequency distribution of high and low flows**

212 In order to evaluate the usefulness of the information provided by the one-month-lag seasonal correlation
213 for flow signatures in HFS and LFS, we perform a real-time updating of the frequency distribution of high
214 and low flows based on the average river flow in the previous month. A similar analysis for the high flows
215 was carried out by Aguilar et al. (2017) for the Po and Danube Rivers. In principle, this is a data
216 assimilation approach, since real-time information, i.e. observations of the average river flow, is used in
217 order to update a probabilistic model and inform the forecast of the flow signature of the upcoming season.

218 In detail, a bi-variate meta-Gaussian probability distribution (Kelly and Krzysztofowicz, 1997;
219 Montanari and Brath, 2004) is fitted between the observed flow signatures, i.e., peak flow in the HFS, Q_P
220 and average flow in the LFS, Q_L , and the average flow in the pre-HFS and LFS months, Q_m , respectively.
221 The peak HFS flow and the average LFS flow are the dependent variables and are extracted as the peak

222 river discharge observed in the previously identified HFS and the average river discharge observed in the
 223 previously identified LFS, respectively. The average flow in the month preceding the HFS and the LFS is
 224 the explanatory variable in both cases. In the following, random variables are denoted by underscore and
 225 their outcomes are written in plain form.

226 The normal quantile transform, NQT (Kelly and Krzysztofowicz, 1997), is used in order to make the
 227 marginal probability distribution of dependent and explanatory variables Gaussian. This is achieved as
 228 follows: a) the sample quantiles Q are sorted in increasing order e.g. $Q_{m_1}, Q_{m_2} \dots Q_{m_n}$, b) the cumulative
 229 frequency, e.g. FQ_{m_i} is computed via a Weibull plotting position, and c) the standard normal quantile, e.g.,
 230 NQ_{m_i} is obtained as the inverse of the standard normal distribution for each cumulative frequency, e.g.,
 231 $G^{-1}(FQ_{m_i})$. Therefore, all sample quantiles are discretely mapped into the Gaussian domain. To get the
 232 inverse transformation for any normal quantile, we connect the points in the above mapping with linear
 233 segments. The extreme segments are extended to allow extrapolation outside the range covered by the
 234 observed sample.

235 In the Gaussian domain, a bivariate Gaussian distribution is fitted between the random explanatory
 236 variable \underline{NQ}_m and the dependent variables \underline{NQ}_P and \underline{NQ}_L by assuming stationarity and ergodicity of the
 237 variables. We define the generic random variable \underline{NQ}_{fs} to represent any dependent flow signature, i.e.; \underline{NQ}_P
 238 and \underline{NQ}_L in our case. Then, the predicted signature at time t can be written as:

$$239 \quad \underline{NQ}_{fs}(t) = \rho(\underline{NQ}_m, \underline{NQ}_{fs}) \underline{NQ}_m(t - h) + N\varepsilon(t) \quad (2)$$

240 where $\rho(\underline{NQ}_m, \underline{NQ}_{fs})$ is the Pearson's cross correlation coefficient between \underline{NQ}_m and \underline{NQ}_{fs} , h is the selected
 241 correlation lag with $h = 1$ in the present application, and $N\varepsilon(t)$ is an outcome of the stochastic process $\underline{N\varepsilon}$,
 242 which is independent, homoscedastic, stochastically independent of \underline{NQ}_m and normally distributed with
 243 zero mean and variance $1 - \rho^2(\underline{NQ}_m, \underline{NQ}_{fs})$. Then, the joint bivariate Gaussian probability distribution
 244 function is defined by the mean ($\mu(\underline{NQ}_m) = 0$ and $\mu(\underline{NQ}_{fs}) = 0$), the standard deviation ($\sigma(\underline{NQ}_m) = 1$ and
 245 $\sigma(\underline{NQ}_{fs}) = 1$) of the standardized normalized series, and the Pearson's cross correlation coefficient between
 246 the normalized series, $\rho(\underline{NQ}_m, \underline{NQ}_{fs})$. From the Gaussian bivariate probability properties, it follows that for

247 any observed $NQ_m(t - h)$ the probability distribution function of $\underline{NQ}_{fs}(t)$ conditioned on NQ_m is Gaussian,
248 with parameters given by:

$$249 \mu(\underline{NQ}_{fs}(t)) = \rho(\underline{NQ}_m, \underline{NQ}_{fs}) NQ_m(t - h) \quad (3)$$

$$250 \sigma(\underline{NQ}_{fs}(t)) = (1 - \rho^2(\underline{NQ}_m, \underline{NQ}_{fs}))^{0.5} \quad (4)$$

251 To derive the probability distribution of $\underline{Q}_{fs}(t)$ conditioned to the observed $Q_m(t - h)$, we first apply the
252 inverse NQT, i.e., we use linear segments to connect the points of the previous discrete quantile mapping of
253 the original quantiles into the Gaussian domain, and accordingly, obtain $Q_{fs}(t)$ for any $\underline{NQ}_{fs}(t)$.
254 Subsequently, we estimate the parameters of an assigned probability distribution for the obtained quantiles
255 in the untransformed domain. This is referred to as the updated probability distribution of the considered
256 flow signature (\underline{NQ}_P and \underline{NQ}_L in our case). We use the Extreme Value Type I distribution for the peak
257 flows and calculate the differences in the magnitude of estimated maxima for a given return period between
258 the unconditioned and the updated distribution. The latter is conditioned by the 95% sample quantile of the
259 observed mean flow in the previous month. To model the low flows we use the lognormal distribution,
260 which was found to exhibit the best fit for the river in question among other typical candidates for average
261 flows, i.e. the Weibull and the Gamma distribution. The low flows are conditioned by the lower 5% sample
262 quantile of the observed mean flow in the previous month.

263 3. Data and catchments description

264 The dataset includes 224 records spanning more than 50 years of daily river flow observations from
265 gauging stations, mostly from non-regulated streams. A few catchments are impacted by regulation.
266 Among the 224 rivers, 108 are located in Austria, 69 in Sweden, 31 in Slovenia, 13 in France, 2 in Spain
267 and one in Italy. Catchment areas vary significantly, the largest being the Po River basin in Italy (70 091
268 km²) and the smaller being the Hålabäck River basin in Sweden (4.7 km²). The geographical location of the
269 river gauge stations as well as their climatic classification are shown in Fig. 1. Most of the examined rivers
270 belong to either a warm temperate (C) or a boreal/snow climate (D) with a subset impacted by polar
271 climatic conditions (E), according to the updated World Map of the Köppen-Geiger climate classification

272 (Fig. 1) based on gridded temperature and precipitation data for the period 1951-2000 (Kottek et al., 2006).
273 More specifically, the majority of French, Slovenian and approximately one third of the Swedish basins
274 belong to the warm temperate Cfb category characterized by precipitation distributed throughout the year
275 (fully humid) and warm summers. The rest of the Swedish catchments are impacted by a Dfc climatic type,
276 i.e. a snow climate, fully humid with cool summers. The Austrian catchments belonging to the region
277 impacted by the European Alps have the most complicated regime due to their topographic variability. At
278 the lowest altitudes, Cfb is the prevailing regime, but as proximity to the Alps increases, a Dfc regime
279 dominates and progressively, in the highest altitude basins, the climate becomes a polar tundra type (Et),
280 characterized primarily by the very low temperatures present. The characteristics of all the climatic regimes
281 of the studied rivers are given in the legend of Fig. 1. A summary of the river basins under study in terms of
282 the selected descriptors is also provided in Table 1, showing that the investigated rivers cover a wide range
283 of catchment area sizes, flow regimes and climatic conditions.

284 It is relevant to note that 16 of the Austrian rivers are subject to regulation, which may alter the
285 persistence properties of river flows. This relates to generally ‘mild’ forms of regulation, i.e. upstream
286 regulation with very low degree of flow attenuation, hydropower operations and flow diversions to and
287 from the basin. A preliminary examination of these rivers did not reveal any significant change during time
288 of the flow regime. The presence of regulation does not preclude the exploitation of correlation for
289 predicting river flows in probabilistic terms, but may affect the analysis of physical drivers, as it may
290 enhance or reduce persistence in the natural river flow regime. Given that detailed information is generally
291 lacking on the impact of regulation (Kuentz et al. 2017), we assume stationarity of the river flows for all the
292 catchments herein considered and additionally, assume that river management does not significantly affect
293 the identification of the physical drivers.

294

295 **4. River memory analysis for the considered case studies**

296 **4.1 Season Identification**

297 Approximately half of the 224 rivers are characterized by at least one high-flow season with medium or
298 higher significance ($\text{PAMF(HFS)} \geq 60\%$). Among them, very strong unimodal regimes ($\text{PAMF(HFS)} \geq$
299 80%) are observed in 63 rivers, the majority of which are located in Sweden. For 25% of the rivers, a high-
300 flow season of low significance is found (PAMF(HFS) between 40–60%), while for the remaining 25% the
301 high-flow distribution looks uniform along the year. Bi-modality regimes are found with low and moderate
302 significance in rivers located mostly in Austria and Sweden, but we focus here on the major high-flow
303 season, as we are interested in the most extreme events. A minor HFS analysis would be perhaps relevant
304 in other regions of the world where bimodal flood regimes are more prominent, as suggested by the
305 analysis of Lee et al. (2015).

306 Regarding the LFS identification, the two considered approaches (see Section 2.1) agree for 139 out
307 of 224 stations but the first method, i.e. the one-month period with the lowest amount of mean monthly
308 flow is selected as being more relevant to the purpose of computing mean flow correlations.

309 **4.2 Seasonal correlation**

310 LFS correlation is markedly higher than the corresponding HFS correlation for lags 1–5 and its median
311 remains higher than 0 for more lags (see Fig. 2). For the case of HFS correlation, we focus only on the most
312 significant first lag, for which 73 rivers are found to have correlation significantly higher than 0 at 5%
313 significance level. In Fig. 3, the autocorrelation of the whole monthly series is compared to the LFS
314 correlation for lag of 1 and 2 months, in order to prove that the seasonal correlation for LFS is significantly
315 higher than its counterpart computed by considering the whole year. The latter is also confirmed by the
316 Kolmogorov-Smirnov test for both LFS lags (corresponding p-values, $p_{\text{lag1}} < 2.2 \times 10^{-6}$ and $p_{\text{lag2}} < 2.2 \times 10^{-6}$
317 for the null hypothesis that the LFS correlation coefficients are not higher than the corresponding values for
318 the monthly series autocorrelation; Conover, 1971).

319 Figure 4 shows the spatial pattern of HFS and LFS streamflow correlations. It is interesting to notice
320 the emergence of spatial clustering in the correlation magnitude, which implies its dependence on different
321 spatially varying physical mechanisms. For example, for HFS, a geographical pattern emerges within
322 France, since the highest correlation coefficients are located in the northern part of the country, which is
323 characterized by oceanic climate and higher baseflow indexes.

324 **5. Physical interpretation of correlation**

325 To attribute the detected correlations to physical drivers, we define 6 groups of potential drivers of seasonal
326 correlation magnitude, which are: basin size, flow indices, presence of lakes and glaciers, catchment
327 elevation, catchment geology, and hydro-climatic forcing. For some of the descriptors the information is
328 available for a few countries only.

329 In what follows, we will use the term “positive (negative) impact on correlation” to imply that an
330 increasing value of the considered descriptor is associated to increasing (decreasing) correlation. For each
331 descriptor, we also report between parentheses the Spearman’s rank correlation coefficient r_s (Spearman,
332 1904) between its value and the considered (LFS or HFS) correlation, and the p-value of the null
333 hypothesis $r_s = 0$. Spearman’s coefficient is adopted in view of its robustness to the presence of outliers and
334 its capability of capturing monotonic relationships of non-linear type.

335 **5.1 Catchment area – Descriptor A**

336 Figure 5 shows that there is only a weak positive impact of the catchment area (log-transformed) on
337 correlation for HFS ($r_s = 0.17$, $p = 0.01$) but a more significant positive one for LFS ($r_s = 0.27$, $p = 5.5 \times 10^{-5}$).
338 The presence of relevant scatter in the plots also indicates that it is not a key determinant of correlation.

339 **5.2 Flow indices – Descriptors BI and SR**

340 The effect of the BI and SR is shown in Fig. 6. BI (Fig. 6a) appears to be a marked positive driver for LFS
341 ($r_s = 0.6$, $p = 1.8 \times 10^{-23}$) while its effect for HFS is less clear, being weakly positive ($r_s = 0.21$, $p = 0.001$).

342 For SR (Fig. 6b), it appears that both LFS and HFS streamflow correlations drop for increasing wetness (r_s
343 $= -0.4$, $p = 4 \times 10^{-10}$ and $r_s = -0.28$, $p = 2.8 \times 10^{-5}$ respectively).

344 **5.3 Presence of lakes and glaciers – Descriptors PL and PG**

345 Detailed information on the presence of lakes is available for the 69 Swedish catchments while areal
346 extension of glaciers is known for the 108 Austrian catchments. Figure S1 in the Supplement shows that the
347 impact of lake area (Fig. S1a) on correlation for LFS and HFS is not significant but positive ($r_s = 0.10$, $p =$
348 0.399 and $r_s = 0.12$, $p = 0.347$). The results for glaciers show a positive impact for LFS ($r_s = 0.28$, $p =$
349 0.081) but negative for HFS ($r_s = -0.34$, $p = 0.032$). For a meaningful interpretation, these results should be
350 considered in conjunction with the seasonality of flows for the Austrian catchments. Low flows for the
351 glacier-dominated catchments are typically occurring in winter months, when glaciers are not contributing
352 to the flow (Parajka et al., 2009). Thus the observed result for LFS is more likely portraying the impact of
353 low temperature (low evapotranspiration) and snow accumulation, the latter generally being a slowly
354 varying process. For HFS, which is typically occurring in the summer months for the considered
355 catchments, flows are mainly determined by snowmelt which is associated to large variability and reduced
356 persistence (Fig. S1b).

357 **5.4 Catchment elevation**

358 The areal coverage of the SRTM data is limited to 60 degrees north and 54 degrees south and therefore,
359 data for the northern part of the Swedish catchments are not available. The rest of the rivers are divided in
360 three regions based on proximity: Region I including the central and eastern part of the Alps and
361 encompassing Austrian, Slovenian and Italian catchments; Region II showing the western part of the Alps
362 and encompassing French and Spanish territory; and Region III including the southern part of Sweden.
363 Figure 8 shows elevation maps along with the location of gauge stations and magnitude of correlations.
364 Elevation seems to enhance LFS correlation which is more evident in the mountainous Region I (Fig. 7).
365 For HFS correlation there is not a prevailing pattern.

366 In the case of Austrian catchments, a 1 km resolution digital model is also used to extract information
367 on elevation. Figure 8 confirms that there is a positive correlation pattern emerging with elevation for LFS.
368 Based on local climatological information, it can be concluded that the spatial pattern for LFS correlation is
369 reflective of the timing and strength of seasonality of the low flows in Austria, where dry months occur in
370 lowlands during the summer due to increased evapotranspiration and in the mountains during winter
371 (mostly February) due to snow accumulation which is characterised by stronger seasonality compared to
372 the lowlands flow regime (Parajka et al., 2016; see Fig. 1). Concerning HFS in the same region, high flows
373 are significantly impacted by the seasonality of extreme precipitation (Parajka et al., 2010), which is highly
374 variable, with the exception of the rivers where high flows are generated by snowmelt. Therefore, a
375 spatially consistent pattern does not clearly emerge.

376

377 **5.5 Catchment geology – Descriptors PK and PF**

378 Two different geological behaviours are identified which may impact river correlation. We first focus on 21
379 Slovenian catchments (out of 31) where more than 50% of the basin area is characterised by the presence of
380 karstic aquifers (percentage of karstic areas $PK \geq 50\%$). Figure 9 shows boxplots of the estimated lag-1
381 correlation coefficient for both HFS and LFS against rivers where $PK < 50\%$. It is clear that there is a
382 significant decrease in correlation where karstic areas dominate for both for HFS and LFS.

383 In a second analysis, we focus on Austrian catchments and investigate the relationship between
384 correlation and percentage of Flysch coverage, PF. Figure S2 in the Supplement shows that there is not a
385 prevailing pattern in either case ($r_s = 0.13$, $p = 0.6$ for LFS and $r_s = -0.19$, $p = 0.446$ for HFS).

386 **5.6 Atmospheric forcing – Descriptors P and T**

387 Figure 10 shows the lag-1 HFS and LFS correlations against estimates of the annual precipitation P and
388 annual mean temperature T as well as the De Martonne index IDM. LFS correlation appears to be more
389 sensitive than HFS to the above climatic indices, showing a decrease with increasing temperature and also a

390 decrease with increasing precipitation ($r_s = -0.44$, $p = 3.1 \times 10^{-12}$ for P and $r_s = -0.57$, $p = 1.8 \times 10^{-20}$ for
391 T). HFS correlation is scarcely sensitive to these variables ($r_s =$
392 -0.17 , $p = 0.011$ for P and $r_s = 0.08$, $p = 0.208$ for T). The IDM (Fig. 10 c) shows a mild decrease of both
393 LFS ($r_s = -0.06$, $p = 0.368$) and HFS correlation with increasing IDM ($r_s = -0.17$, $p = 0.01$), while for the
394 latter there seems to be a clearer trend (lower correlation with higher IDM) in very humid areas (dark blue
395 points in Fig. 10c).

396

397 **5.7 Physical drivers of high correlation**

398 To gain further insights into the results we select the 20 catchments with the highest streamflow seasonal
399 correlation coefficients for both HFS and LFS periods in order to investigate their physical characteristics
400 in relation to the remaining set of rivers. Table 2 summarizes statistics for selected descriptors in order to
401 identify dominant behaviours. We also compare the number of rivers with distinctive features, i.e. lakes N_L
402 (number of rivers with lakes), glaciers N_G (number of river with glaciers), flysch N_F (number of rivers with
403 flysch formations) and karst N_K (number of rivers with karstic areas) for the highest correlation group with
404 those obtained from 1000 randomly sampled 20-catchment groups from the whole set of considered
405 catchments to assess whether higher correlation implies distinctive features.

406 By focusing on HFS, one can notice that the catchments with higher seasonal correlation are
407 characterised by larger catchment area, higher baseflow index and temperature with respect to the
408 remaining catchments, and lower specific runoff, precipitation and wetness. Presence of lake, glaciers,
409 karstic and Flysch areas do not appear significantly effective at a 5% significance level. More robust
410 considerations can be drawn for the LFS: higher seasonal correlation is found for larger catchments with
411 higher baseflow index and lower specific runoff, precipitation and wetness. Decreasing temperature is
412 strongly associated with higher correlation for the LFS. The presence of lakes plays a significant role both
413 for lag-1 and lag-2 correlations with the latter being also significantly influenced by presence of glaciers.

414 **6. Principal component analysis of the predictors and linear regression**

415 We attempt to fit a linear regression model to relate correlation to physical drivers, in order to support
416 correlation estimation for ungauged catchments. To avoid the impact of multicollinearity in the regression
417 while additionally summarizing river information, we apply PCA (see Section 2.2). Although correlation
418 effects are efficiently dealt with via the PCA, we avoid including highly correlated variables in the analysis.
419 For example, the De Martonne Index, Precipitation and SR are mutually highly correlated (all Pearson's
420 cross-correlations are higher than 0.6) and therefore we only consider the SR in the PCA because it shows a
421 more robust linear relationship with correlation magnitude. We select A , BI , SR and T as the variables to be
422 considered in the PCA. A log transformation is applied on the basin area to reduce impact of outliers. Table
423 3 shows the coefficients estimated for each component (the loadings) and the explained variance. The first
424 principal component is primarily a measure of BI ; the second principal component mostly accounts for T
425 and the third principal component accounts for A . There is an evident geographical pattern emerging by the
426 visualization of countries in the biplot (Fig. 11). Slovenian rivers cluster towards the direction of increasing
427 SR and T , whereas Swedish rivers towards the opposite direction of increasing BI and decreasing T .
428 Austrian rivers, which are the majority, are the most diverse. The first two components together explain the
429 70% of the total variability in the data.

430 Naturally, the statistical behaviour of the indices reflects the known local controls for certain rivers.
431 For example, the observed lowest BI in Slovenia is consistent with the presence of karstic formations for
432 the majority of the Slovenian rivers, as is the higher BI in Sweden and Austria, which is related to the
433 presence of lakes and glaciers in both countries.

434 In the case of HFS, all the examined linear models (combinations of $\ln A$, SR , BI , P , T , IDM
435 predictors) failed in explaining the streamflow correlation magnitude. On the contrary, the linear regression
436 model performs fairly well in explaining the correlation for LFS, with an adjusted R^2 value of 0.58 and an
437 F-test returning a p-value $< 2.2 \times 10^{-16}$. The coefficients for the first three PCs are found significantly
438 different from zero at a 0.1% significance level and are included in the regression (see Table 4). The

439 highest coefficient is obtained for the first PC, which mostly accounts for BI importance. Diagnostic plots
440 from linear regression for LFS are shown in Fig. 12. There is no clear violation of the homoscedasticity
441 assumption in linear regression, apart from the presence of a limited number of outliers. There is a certain
442 departure from normality in the lower tail of the residuals, which relates to the fact that the model performs
443 better in the area of higher seasonal streamflow correlations and overestimates the lower correlations.

444

445 **7. Real-time updating of the frequency distribution of high and low flows for the Oise River**

446 We apply the technical experiment (see section 2.3) for high and low flows to the Oise River in France and
447 assess the difference in the estimated flood and low-flow magnitudes. We update the probability
448 distribution of high and low flows after the occurrence of the upper 95% and lower 5% sample quantile of
449 the observed mean flow in the previous month, respectively.

450 The Oise River (55 years of daily flow values) at Sempigny in France has a basin area of 4320 km² and its
451 gauging station at Sempigny is part of the French national real-time monitoring system
452 (<https://www.vigicrues.gouv.fr/>), which is in place to monitor and forecast floods in the main French rivers.
453 The selected river has a high technical relevance since it experiences both types of extremes with large
454 impacts. For instance, a severe drought event in 2005 led to water restrictions impacting agriculture and
455 water uses in the region (Willsher, 2005), while the river originated an inundation during the 1993 flood
456 events in northern and central France, which was one of the most catastrophic flood-related disasters in
457 Europe in the period 1950-2005 (Barreldo, 2007). It is characterized by HFS correlation $\rho = 0.54$, which is
458 the 3rd largest lag-1 correlation for the HFS in our dataset and LFS correlation $\rho = 0.80$, which stands for
459 the 70% quantile of the sample lag-1 correlation for LFS.

460 A visual inspection of the residuals plots is also performed (Fig. 13a, b) in order to evaluate the
461 assumption of homoscedasticity of the residuals of the regression models given by Eq. (2). The residuals do
462 not show any apparent trend and therefore the Gaussian linear model is accepted. Figure 13 (c, d) shows the
463 conditioned and unconditioned probability distributions of peak and low flows in the Gaussian domain. As

464 follows from Eq. (3) and (4), the variance of the updated (conditioned) distributions decreases while the
465 mean value increases.

466 After application of the inverse NQT the conditioned peak flows are modelled through the EV1
467 distribution and compared to the unconditioned (observed) peak flows. The corresponding Gumbel
468 probability plot for conditioned and unconditioned distributions is shown in Fig. 13e. For the return period
469 of 200 years, the updated distribution shows a 6% increase in the flood magnitude for the Oise River (307.7
470 $\text{m}^3 \text{s}^{-1}$ to $326.44 \text{ m}^3 \text{s}^{-1}$). Likewise, the conditioned low flows are modelled through the lognormal
471 distribution. The two cumulative distribution functions are compared in Fig. 13f showing a major departure
472 in the estimated quantiles for the updated distribution; the occurrence of the predefined 5% quantile flow in
473 the pre-LFS month induces a decrease of the exceedance probability of an average LFS flow of $15 \text{ m}^3 \text{s}^{-1}$
474 from a prior 43% (according to the unconditioned model) to 1%.

475 **8. Discussion**

476 The methodology presented herein aims to progress our physical understanding of seasonal river flow
477 persistence for the sake of exploiting the related information to improve probabilistic prediction of high and
478 low flows. The correlation of average flow in the previous months with LFS flow and HFS peak flow was
479 found to be relevant, with the former prevailing on the latter. This result was foreseen since the LFS
480 correlation refers to average flow while the HFS correlation is related to rapidly occurring events. We also
481 aim to investigate physical drivers for correlation and quantify their relative impact on correlation
482 magnitude. Therefore, a thorough investigation of the geophysical and climatological features of the
483 considered catchments was carried out.

484 We found that increasing basin area and baseflow index are associated with increasing seasonal
485 streamflow correlation, yet the latter has a stronger impact. To this respect, Mudelsee (2007), Hirpa et al.
486 (2010) and Szolgayova et al. (2014a) also found positive dependencies of long-term persistence on basin
487 area, Markonis et al. (2018) found a positive impact too but for larger spatial scales ($> 2 \times 10^4 \text{ km}^2$), while
488 Gudmunsson et al. (2011) found basin area to have negligible to no impact to the low-frequency

489 components of runoff. Our results additionally point out that catchment storage induces mild positive
490 correlation, not only for low discharges which are directly governed by base flow, but also for high flows,
491 which is less anticipated.

492 Previous studies also pointed out that correlation increases for groundwater-dominated regimes
493 (Yossef et al., 2013; Dijk et al., 2013; Svensson, 2016) and slower catchment response times (Bierkens and
494 van Beek, 2009), which concurs with the impact of baseflow index found herein as well as with the
495 observed impact of fast responding karst areas. The latter findings are also in agreement with our
496 conclusion that correlation decreases for increasing rapidity of river flow formation, which for instance
497 occurs in the presence of karstic areas and wet soils, which explains why persistence decreases with high
498 specific runoff; as also confirmed by other studies (Gudmundsson et al., 2011; Szolgayova et al., 2014).

499 Other contributions also reported higher streamflow persistence in drier conditions, either relating to
500 lower specific runoff or mean areal precipitation estimates (Szolgayova et al., 2014; Markonis et al., 2018).
501 It was postulated that this is due to wet catchments showing increased short-term variability compared to
502 drier catchments (Szolgayova et al., 2014) and having a faster response to rainfall due to saturated soil. A
503 similar conclusion has been reached by other previous studies reporting that low humidity catchments are
504 more sensitive to inter-annual rainfall variability (Harman et al., 2011), therefore leading to enhanced
505 persistence. Yet, these studies refer to generally humid regions and cannot be extrapolated to more arid
506 climates. A related conclusion is proposed by Seneviratne et al. (2006) who found the highest soil moisture
507 memory for intermediate soil wetness. These results do not contrast with our findings, which refer to a wide
508 range of climatic conditions. In fact, our finding that increased wetness has a negative impact on seasonal
509 memory of both high and low flows, extends the above results to the seasonal scale and interestingly, to
510 both types of extremes.

511 We also confirm the role of lakes in determining higher catchment storage and therefore positive
512 correlations for the LFS, which has only been reported for annual persistence in a few sites (Zhang et al.,
513 2012).

514 The effect of snow cover for lag-1 LFS correlation is also revealed by the Austrian catchments. The
515 mountainous rivers, directly affected by the process of snow accumulation, exhibit winter LFS and higher
516 correlation than the rivers in the lowlands, which are more prone to drying out due to evapotranspiration in
517 the hotter summer months. The inspection of elevation data confirmed the role of high altitudes in
518 increasing LFS correlation, which is likely related to storage effects due to snow accumulation and gradual
519 melting. In this respect, Kuentz et al. (2017) found that topography exerts dominant controls over the flow
520 regime in the larger European region, controlling the flashiness of flow, and being a particularly important
521 driver for other low flow signatures too. In fact, topography may affect the flow regime directly, through
522 flow routing, but also indirectly, because of orographic effects in precipitation and hydroclimatic processes
523 affected by elevation (e.g. snowmelt and evapotranspiration).

524 Regarding atmospheric forcing, we find LFS correlation to be negatively correlated to mean areal
525 temperature and annual precipitation. The former result may be explained considering that increased
526 evapotranspiration (higher temperature) is likely to dry out LFS flows while snow coverage (lower
527 temperature) was found to be associated with higher LFS correlation. An apparently different conclusion
528 was drawn by Szolgayova et al. (2014a) and Gudmundsson et al. (2011), who reported increasing
529 persistence with increasing mean temperature postulating that snow-dominated flow regimes smooth out
530 interannual fluctuations. Yet, it should be noted that they refer to interannual variability while we refer here
531 to seasonal correlation and therefore to shorter time scales, which imply a different dynamic of snow
532 accumulation and snowmelt; latitude may also play a relevant role in this, since in southern Europe the
533 complete ablation of snow can occur more than once during the cold season, and sublimation may account
534 for 20–30% of the annual snowfall (Herrero and Polo, 2016), decreasing the amount of snowmelt and
535 impacting LFS flows in the summer season.

536 Snowmelt mechanisms are found to increase predictive skill during low-flow periods in some other
537 studies (Bierkens and van Beek, 2009; Mahanama et al., 2011; Dijk et al., 2013). However, in the glacier-
538 dominated regime of western Alpine and central Austrian catchments, it is unlikely that this is a relevant

539 driver of higher correlation, since low flow is occurring in the winter months. Yet the mountainous, glacier-
540 dominated rivers still show increased LFS correlation compared to rivers in the lowlands, which agrees
541 well with other studies that have found less uncertainty in the rainfall-runoff modelling in this regime
542 owing to the greater seasonality of the runoff process and the decreased impact of rainfall compared to the
543 rainfall-dominated regime of the lowlands (e.g Parajka et al., 2016).

544 Although the considerable uncertainty of areal precipitation estimates should be acknowledged, the
545 contribution of annual precipitation interestingly complements the negative effect of increasing specific
546 runoff –which is highly correlated to P estimates– on the correlation magnitude for both LFS and HFS.
547 This outcome confirms that catchments receiving significant amount of rainfall do show less correlation
548 than drier regimes as discussed before.

549

550 **9. Conclusions and outlook**

551 This research investigates the presence of persistence in river flow at the seasonal scale, the associated
552 physical drivers and the prospect for employing the related information to improve probabilistic prediction
553 of high and low flows by exploring a large sample of European rivers. The main findings are summarized
554 below:

- 555 • Rivers in Europe show persistent features at the seasonal timescale, manifested as correlation between
556 high- and low-flow signatures, i.e. peak flows in HFS and average flows in LFS respectively, and
557 average flows in the previous month. Correlation for LFS signatures is found consistently higher than
558 HFS.
- 559 • Seasonal correlation shows increased spatial variability together with spatial clustering.
- 560 • Storage mechanisms, groundwater-dominated basins and slower catchment response time, as reflected
561 by large basin areas, high baseflow index and the presence of lakes, amplify seasonal correlation. On

562 the contrary, correlation is lower in quickly responding karstic basins, and increased wetness
563 conditions, as revealed by high specific runoff.

- 564 • Low mean areal temperature is associated with higher LFS correlation owing to the weaker drying-out
565 evapotranspiration force and the mechanism of snow accumulation in higher altitudes. Higher mean
566 areal precipitation is associated with lower LFS predictability, possibly due to the presence of saturated
567 conditions and increased short-term variability in wetter climates.
- 568 • The drivers of LFS predictability are easier to identify and allow for the opportunity to construct
569 regression models for possible application to ungauged basins (see Section 6).
- 570 • HFS and LFS correlation may directly serve for the probabilistic prediction of ‘extremes’, i.e. high and
571 low flows, as increased correlation can be exploited in various stochastic models. Such an application
572 was performed in Section 7 in a data assimilation setting for a river of marked technical relevance.

573 Regarding the latter, once a significant correlation is identified, it may be exploited in other model
574 variants as well, e.g. adding more dependent variables of lagged flow and/or coupling with other relevant
575 explanatory variables, such as teleconnections or antecedent rainfall, in multivariate prediction schemes.
576 Indeed, the presence of river memory at the seasonal scale represents a possible opportunity to improve the
577 prediction of water-related natural hazards by reducing uncertainty of associated estimates and allowing
578 significant lag time for decision-making and hazard prevention. Besides the high relevance for extremes,
579 this type of seasonal predictability could also be of interest to water resources management by, for instance,
580 exploring the memory properties of a minor HFS.

581 The inspection of the physical basis, apart from advancing our understanding of the catchment
582 dynamics and enabling predictions in ungauged basins, is highly important as it may guide the search for
583 other dependent variables and build confidence in the formation of process-based stochastic models
584 (Montanari and Koutsoyiannis, 2012). A large sample of indices was herein inspected, yet data are majorly
585 needed to allow for more certain and generalized conclusions worldwide. An important note is the presence
586 of regulation, the effect of which, due to lack of objective data, is not completely understood. However, the

587 opportunity of exploiting correlation is not affected by the presence of regulation, provided that the
588 management of river flow does not change in time.

589 We conclude that our results point out that river memory provides interesting information that holds
590 both theoretical and operational potential to improve the understanding and prediction of extremes, support
591 decision-making and increase the level of preparedness for water-related natural hazards.

592 **Data and Code availability**

593 The data and code used in this study may be made available to the readers upon request to the
594 corresponding author.

595 **Competing interests**

596 The authors declare that they have no conflict of interest.

597 **Acknowledgements**

598 The present work was (partially) developed within the framework of the Panta Rhei Research Initiative of
599 the International Association of Hydrological Sciences (IAHS). Part of the results were elaborated in the
600 Switch-On Virtual Water Science Laboratory that was developed in the context of the SWITCH-ON
601 (Sharing Water-related Information to Tackle Changes in the Hydrosphere – for Operational Needs)
602 project, funded by the European Union Seventh Framework Programme (FP7/2007-2013) under grant
603 agreement no. 603587. N. Bezak gratefully acknowledges funding by the Slovenian Research Agency
604 (grants J2-7322 and P2-0180). M. Bermúdez gratefully acknowledges financial support from the Spanish
605 Regional Government of Galicia, Postdoctoral Grant Program 2014.

606 **References**

607 Aguilar, C., Montanari, A., and Polo, M.-J.: Real-time updating of the flood frequency distribution through
608 data assimilation, *Hydrol. Earth Syst. Sci.*, 21, 3687–3700, [https://doi.org/10.5194/hess-21-3687-](https://doi.org/10.5194/hess-21-3687-2017)
609 [2017](https://doi.org/10.5194/hess-21-3687-2017), 2017.

- 610 Barredo, J.I.: Major flood disasters in Europe: 1950–2005, *Nat. Hazards*, 42, 125–148,
611 <https://doi.org/10.1007/s11069-006-9065-2>, 2007.
- 612 Bierkens, M.F.P., and van Beek, L.P.H.: Seasonal Predictability of European Discharge: NAO and
613 Hydrological Response Time, *J. Hydrometeorol.*, 10, 953–968,
614 <https://doi.org/10.1175/2009JHM1034.1>, 2009.
- 615 Cervi, F., Blöschl, G., Corsini, A., Borgatti, L., and Montanari, A.: Perennial springs provide information to
616 predict low flows in mountain basins, *Hydrolog. Sci. J.*, 62, 2469–2481,
617 <https://doi.org/10.1080/02626667.2017.1393541>, 2017.
- 618 Chiew, F.H.S., Zhou, S.L., and McMahon, T.A.: Use of seasonal streamflow forecasts in water resources
619 management, *J. Hydrol.*, 270, 135–144, [https://doi.org/10.1016/S0022-1694\(02\)00292-5](https://doi.org/10.1016/S0022-1694(02)00292-5), 2003.
- 620 Conover, W.J.: *Practical Nonparametric Statistics*, New York: John Wiley and Sons. Inc, 1971.
- 621 Cunderlik, J.M., Ouarda, T.B., and Bobée, B.: Determination of flood seasonality from hydrological
622 records/Détermination de la saisonnalité des crues à partir de séries hydrologiques, *Hydrolog. Sci. J.*,
623 49, <https://doi.org/10.1623/hysj.49.3.511.54351>, 2004.
- 624 De Martonne, E.M.: L'indice d'aridité. *Bulletin de l'Association de géographes français* 3, 3–5,
625 <https://doi.org/10.3406/bagf.1926.6321>, 1926.
- 626 Dijk, A.I., Peña-Arancibia, J.L., Wood, E.F., Sheffield, J., and Beck, H.E.: Global analysis of seasonal
627 streamflow predictability using an ensemble prediction system and observations from 6192 small
628 catchments worldwide, *Water Resour. Res.*, 49, 2729–2746, <https://doi.org/10.1002/wrcr.20251>,
629 2013.
- 630 Dimitriadis, P., Koutsoyiannis, D., and Tzouka, K.: Predictability in dice motion: how does it differ from
631 hydro-meteorological processes?, *Hydrolog. Sci. J.*, 61, 1611–1622,
632 <https://doi.org/10.1080/02626667.2015.1034128>, 2016.
- 633 Gabriel, K.R.: The biplot graphic display of matrices with application to principal component analysis,
634 *Biometrika* 58, 453–467, <https://doi.org/10.1093/biomet/58.3.453>, 1971.
- 635 Gower, J.C., and Hand, D.J.: *Biplots*, CRC Press, 1995.
- 636 Gudmundsson, L., Tallaksen, L.M., Stahl, K., and Fleig, A.K.: Low-frequency variability of European
637 runoff, *Hydrol. Earth Syst. Sci.*, 15, 2853–2869, <https://doi.org/10.5194/hess-15-2853-2011>, 2011.
- 638 Gustard, A., and Demuth, S.: *Manual on low-flow estimation and prediction*, Opera, 2009.
- 639 Harman, C.J., Troch, P.A., and Sivapalan, M.: Functional model of water balance variability at the
640 catchment scale: 2. Elasticity of fast and slow runoff components to precipitation change in the
641 continental United States, *Water Resour. Res.*, 47, <https://doi.org/10.1029/2010WR009656>, 2011.
- 642 Herrero, J., and Polo, M.J.: Evaporsublimation from the snow in the Mediterranean mountains of Sierra
643 Nevada (Spain), *The Cryosphere*, 10, 2981–2998, <https://doi.org/10.5194/tc-10-2981-2016>, 2016.
- 644 Hirpa, F.A., Gebremichael, M., and Over, T.M.: River flow fluctuation analysis: Effect of watershed area,
645 *Water Resour. Res.*, 46, <https://doi.org/10.1029/2009WR009000>, 2010.
- 646 Hurst, H.E.: Long-term storage capacity of reservoirs, *Trans. Amer. Soc. Civil Eng.*, 116, 770–808, 1951.
- 647 Jolliffe, I.: *Principal component analysis*, Wiley Online Library,
648 <https://doi.org/10.1002/9781118445112.stat06472>, 2002.
- 649 Kelly, K.S., and Krzysztofowicz, R.: A bivariate meta-Gaussian density for use in hydrology, *Stoch.*
650 *Hydrol. Hydraul.*, 11, 17–31, <https://doi.org/10.1007/BF02428423>, 1997.
- 651 Kotteck, M., Grieser, J., Beck, C., Rudolf, B., and Rubel, F.: World Map of the Köppen-Geiger climate
652 classification updated, *Meteorologische Zeitschrift* 259–263, <https://doi.org/10.1127/0941-2948/2006/0130>, 2006.
- 653
- 654 Koutsoyiannis, D.: Hurst-Kolmogorov Dynamics and Uncertainty, *JAWRA Journal of the American Water*
655 *Resources Association*, 47, 481–495, <https://doi.org/10.1111/j.1752-1688.2011.00543.x>, 2011.
- 656 Koutsoyiannis, D., Yao, H., and Georgakakos, A.: Medium-range flow prediction for the Nile: a
657 comparison of stochastic and deterministic methods/Prévision du débit du Nil à moyen terme: une
658 comparaison de méthodes stochastiques et déterministes, *Hydrolog. Sci. J.*, 53, 142–164,
659 <https://doi.org/10.1623/hysj.53.1.142>, 2008.

- 660 Kuentz, A., Arheimer, B., Hundecha, Y. and Wagener, T.: Understanding hydrologic variability across
661 Europe through catchment classification, *Hydrol. Earth Syst. Sci.*, 21(6), p.2863-2879,
662 <https://doi.org/10.5194/hess-21-2863-2017>, 2017.
- 663 Lee, D., Ward, P., and Block, P.: Defining high-flow seasons using temporal streamflow patterns from a
664 global model, *Hydrol. Earth Syst. Sci.*, 19, 4689-4705, <https://doi.org/10.5194/hess-19-4689-2015>,
665 2015.
- 666 Mahanama, S., Livneh, B., Koster, R., Lettenmaier, D., and Reichle, R.: Soil Moisture, Snow, and Seasonal
667 Streamflow Forecasts in the United States, *J. Hydrometeorol.*, 13, 189–203,
668 <https://doi.org/10.1175/JHM-D-11-046.1>, 2011.
- 669 Markonis, Y., Moustakis, Y., Nasika, C., Sychova, P., Dimitriadis, P., Hanel, M., Máca, P., and Papalexiou,
670 S.M.: Global estimation of long-term persistence in annual river runoff, *Adv. Water Resour.*, 113,
671 1–12, <https://doi.org/10.1016/j.advwatres.2018.01.003>, 2018.
- 672 Montanari, A.: Hydrology of the Po River: looking for changing patterns in river discharge, *Hydrol. Earth*
673 *Syst. Sci.*, 16, 3739–3747, <https://doi.org/10.5194/hess-16-3739-2012>, 2012.
- 674 Montanari, A., and Brath, A.: A stochastic approach for assessing the uncertainty of rainfall-runoff
675 simulations, *Water Resour. Res.*, 40. <https://doi.org/10.1029/2003WR002540>, 2004.
- 676 Montanari, A., and Koutsoyiannis, D.: A blueprint for process-based modeling of uncertain hydrological
677 systems, *Water Resour. Res.*, 48, <https://doi.org/10.1029/2011WR011412>, 2012.
- 678 Mudelsee, M.: Long memory of rivers from spatial aggregation, *Water Resour. Res.*, 43,
679 <https://doi.org/10.1029/2006WR005721>, 2007.
- 680 O’Connell, P.E., Koutsoyiannis, D., Lins, H.F., Markonis, Y., Montanari, A., and Cohn, T.: The scientific
681 legacy of Harold Edwin Hurst (1880–1978), *Hydrolog. Sci. J.*, 61, 1571–1590,
682 <https://doi.org/10.1080/02626667.2015.1125998>, 2016.
- 683 Parajka, J., Blaschke, A.P., Blöschl, G., Haslinger, K., Hepp, G., Laaha, G., Schöner, W., Trautvetter, H.,
684 Viglione, A., and Zessner, M.: Uncertainty contributions to low-flow projections in Austria, *Hydrol.*
685 *Earth Syst. Sci.*, 20, 2085–2101, <https://doi.org/10.5194/hess-20-2085-2016>, 2016.
- 686 Parajka, J., Kohnová, S., Bálint, G., Barbuc, M., Borga, M., Claps, P., Cheval, S., Dumitrescu, A., Gaume,
687 E., Hlavčová, K., and Merz, R.: Seasonal characteristics of flood regimes across the Alpine–
688 Carpathian range, *J. Hydrol.*, 394, 78–89, <https://doi.org/10.1016/j.jhydrol.2010.05.015>, 2010.
- 689 Parajka, J., Kohnová, S., Merz, R., Szolgay, J., Hlavčová, K., and Blöschl, G.: Comparative analysis of the
690 seasonality of hydrological characteristics in Slovakia and Austria/Analyse comparative de la
691 saisonnalité de caractéristiques hydrologiques en Slovaquie et en Autriche, *Hydrolog. Sci. J.*, 54,
692 456–473, <https://doi.org/10.1623/hysj.54.3.456>, 2009.
- 693 Piechota, T.C., Chiew, F.H., Dracup, J.A. and McMahon, T.A.: Development of exceedance probability
694 streamflow forecast, *J. Hydrol. Eng.*, 6(1), pp.20-28, [https://doi.org/10.1061/\(ASCE\)1084-0699\(2001\)6:1\(20\)](https://doi.org/10.1061/(ASCE)1084-0699(2001)6:1(20)), 2001.
- 696 Prudhomme, C., Hannaford, J., Harrigan, S., Boorman, D., Knight, J., Bell, V., Jackson, C., Svensson, C.,
697 Parry, S., and Bachiller-Jareno, N.: Hydrological Outlook UK: an operational streamflow and
698 groundwater level forecasting system at monthly to seasonal time scales, *Hydrolog. Sci. J.*, 62,
699 2753–2768, <https://doi.org/10.1080/02626667.2017.1395032>, 2017.
- 700 Ravbar, N.: Variability of groundwater flow and transport processes in karst under different hydrologic
701 conditions/Spremenljivost Pretakanja Voda in Prenosa Snovi V Krasu ob Razlicnih Hidroloških
702 Pogojih, *Acta Carsologica* 42, 327, <http://dx.doi.org/10.3986/ac.v42i2.644>, 2013.
- 703 Seneviratne, S.I., Koster, R.D., Guo, Z., Dirmeyer, P.A., Kowalczyk, E., Lawrence, D., Liu, P., Mocko, D.,
704 Lu, C.-H., Oleson, K.W., and Verseghy, D.: Soil moisture memory in AGCM simulations: analysis
705 of global land–atmosphere coupling experiment (GLACE) data, *J. Hydrometeorol.*, 7, 1090–1112,
706 <https://doi.org/10.1175/JHM533.1>, 2006.
- 707 Spearman, C.: The Proof and Measurement of Association between Two Things, *The American Journal of*
708 *Psychology*, 15, 72–101, <https://doi.org/10.2307/1412159>, 1904.

709 Svensson, C.: Seasonal river flow forecasts for the United Kingdom using persistence and historical
710 analogues, *Hydrolog. Sci. J.*, 61, 19–35, <https://doi.org/10.1080/02626667.2014.992788>, 2016.

711 Szolgayova, E., Laaha, G., Blöschl, G., and Bucher, C.: Factors influencing long range dependence in
712 streamflow of European rivers, *Hydrol. Process.*, 28, 1573–1586, <https://doi.org/10.1002/hyp.9694>,
713 2014.

714 Wang, Q.J., Robertson, D.E., and Chiew, F.H.S.: A Bayesian joint probability modeling approach for
715 seasonal forecasting of streamflows at multiple sites, *Water Resour. Res.*, 45,
716 <https://doi.org/10.1029/2008WR007355>, 2009.

717 Willsher, K.: France brings in water rationing after worst drought for 30 years, *The Guardian*,
718 <https://www.theguardian.com/environment/2005/jul/11/weather.france>, 2005.

719 Yossef, N.C., Winsemius, H., Weerts, A., Beek, R., and Bierkens, M.F.: Skill of a global seasonal
720 streamflow forecasting system, relative roles of initial conditions and meteorological forcing, *Water*
721 *Resour. Res.*, 49, 4687–4699, <http://dx.doi.org/10.1002/wrcr.20350>, 2013.

722 Zhang, Q., Zhou, Y., Singh, V.P., and Chen, X.: The influence of dam and lakes on the Yangtze River
723 streamflow: long-range correlation and complexity analyses, *Hydrol. Process.* 26, 436–444,
724 <http://dx.doi.org/10.1002/hyp.8148>, 2012.

725
726

727 Tables

728 **Table 1** Summary statistics of the river descriptors. Summary statistics for PL, PG and PF variables are computed
729 only for the subset of catchments with positive values (the total number of catchments is also reported in brackets).
730 PK is used as a categorical variable (PK is either higher or lower than 50% of catchment area), therefore sample
731 statistics are not computed in this case, but the number of stations with $PK \geq 50\%$ is reported as ‘positive’ presence
732 of karst.

Descriptor (Units)	A (km ²)	BI (–)	SR (m ³ s ⁻¹ km ⁻²)	PL (%)	PG (%)	PF (%)	PK (–)	<i>P</i> (mm year ⁻¹)	<i>T</i> (°C)	IDM (–)
Min	4.7	0.29	0.004	0.5	0.1	0.3	–	444	–1.8	29.41
Max	70091	0.99	0.088	19.5	56.5	100	–	1500	13.7	153.40
Standard deviation	5904.3	0.14	0.018	4.04	15.54	32.56	–	288.22	3.59	24.53
Sample size	224	224	224	69 [69]	39 [108]	18 [108]	21 [31]	224	224	224

733

734

735

736

737

738 **Table 2** Differences in the mean values between the descriptors of the 20-highest correlation river group for HFS and
 739 LFS vs the remaining rivers (204). N_L , N_G , N_F and N_K columns contain the absolute number of rivers in the higher
 740 correlation group with the specific descriptor (presence of lake, glacier, flysch and karst) with * denoting
 741 significance at 5% significance level (two-sided test) and brackets containing the mean value from the 1000
 742 resampled 20-catchment subsets.

Descriptor (Units)	A (km ²)	BI (-)	SR (m ³ s ⁻¹ km ⁻²)	N_L (-)	N_G (-)	N_F (-)	N_K (-)	P (mm year ⁻¹)	T (°C)	IDM (-)
HFS lag1	+38.7%	+9.6%	-36.5%	5 [6]	5 [3]	1 [2]	1 [2]	-6.7%	+11.7%	-11.3%
LFS lag1	+358%	+20.2%	-47.3%	17* [6]	3 [3]	0 [2]	0 [2]	-37.9%	-80%	-17.3%
LFS lag2	+139.7%	+18.9%	-40.8%	12* [6]	7* [3]	0 [2]	0 [2]	-26.5%	-64.2%	-8.8%

743

744 **Table 3** Loadings of the three Principal Components for $\ln A$, SR, BI and T . The explained variance of each PC is
 745 denoted in parenthesis.

Predictor variables	PC1 (42.5%)	PC2 (28.2%)	PC3 (17%)	PC4 (12.2%)
$\ln A$	-0.486	-0.427	0.748	0.145
SR	0.48	0.483	0.652	-0.332
BI	-0.619	0.262	-0.11	-0.731
T	0.385	-0.718	-0.04	-0.577

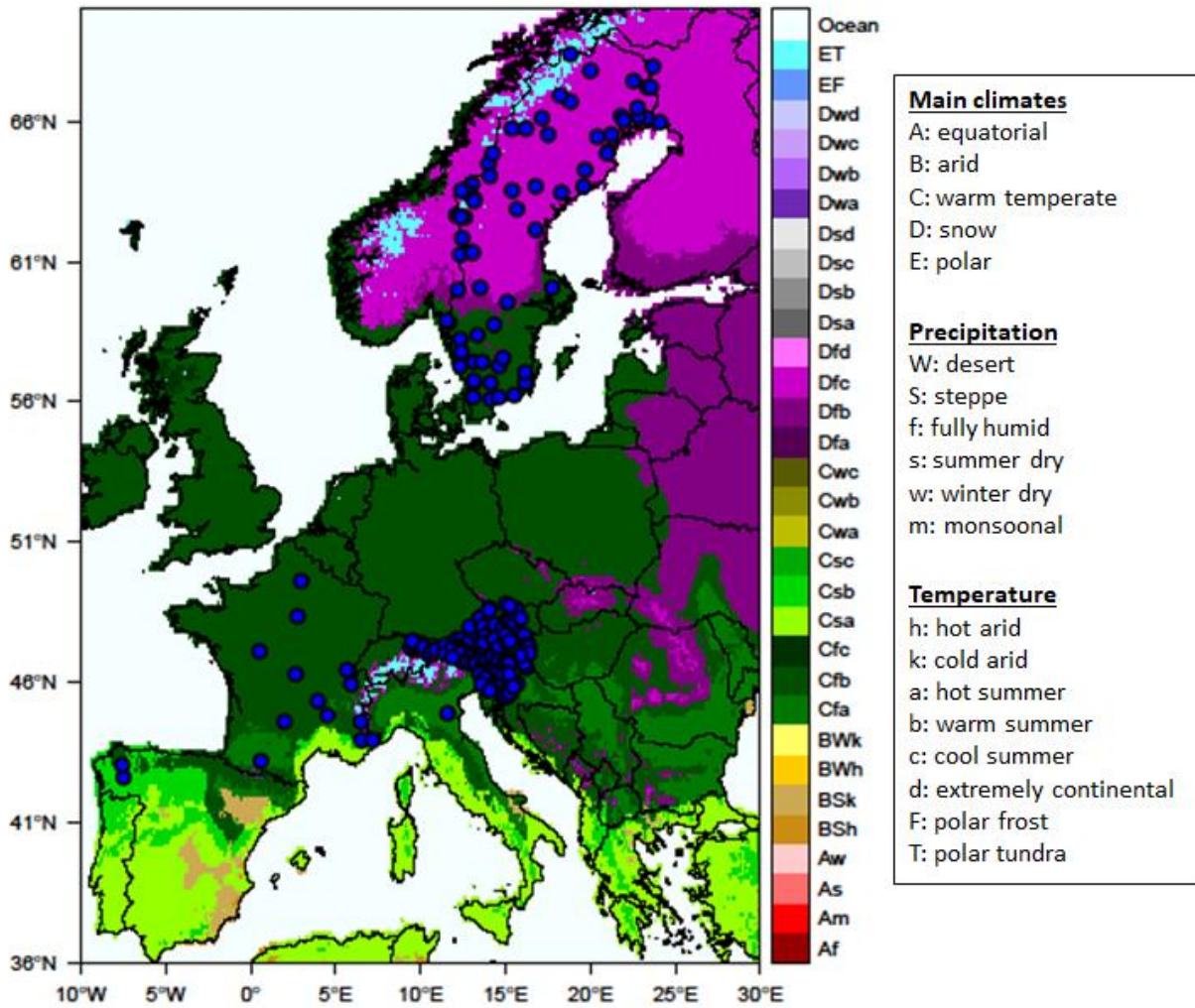
746

747 **Table 4** Summary of Linear Regression results for the LFS model. *** indicate a 0.1% significance level.

Predictor variables	Estimate	Standard Error	t value	Pr(> t)	Adjusted R^2	F-statistic
intercept	0.659407	0.008557	77.065	$< 2 \times 10^{-16}$ ***	0.5834	104.2
PC1	-0.110632	0.006577	-16.820	$< 2 \times 10^{-16}$ ***		p-value:
PC2	0.031761	0.008070	3.936	0.000111***		$< 2.2 \times 10^{-16}$
PC3	-0.038999	0.010388	-3.754	0.000223***		

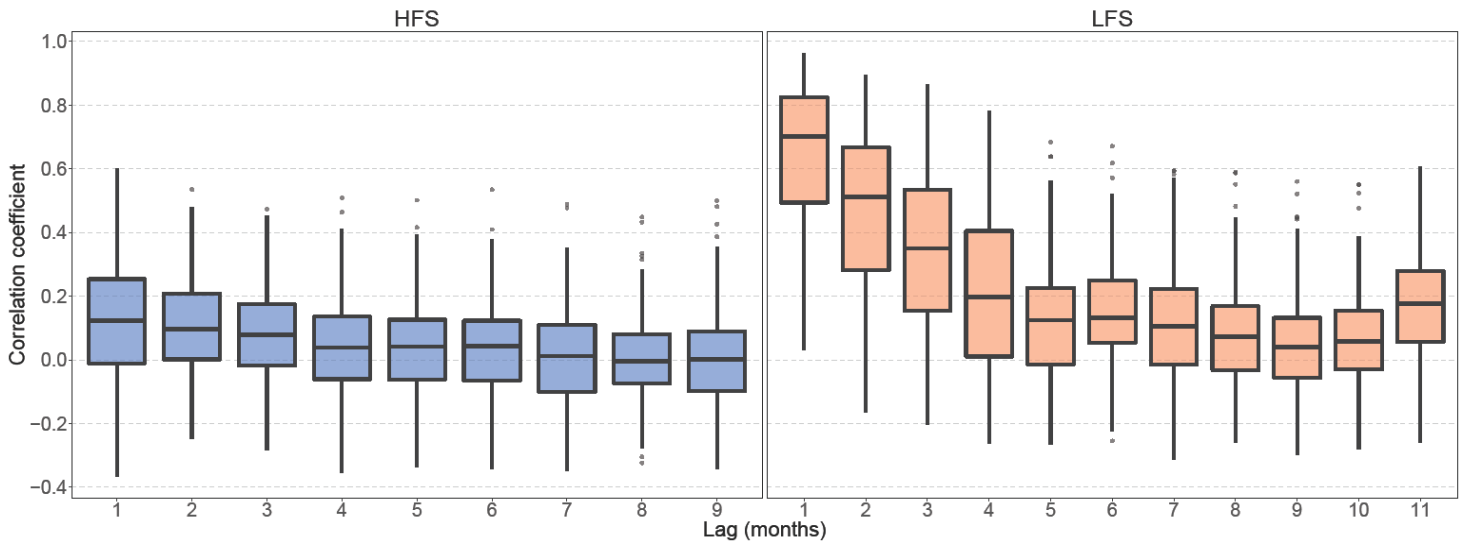
748

749



751

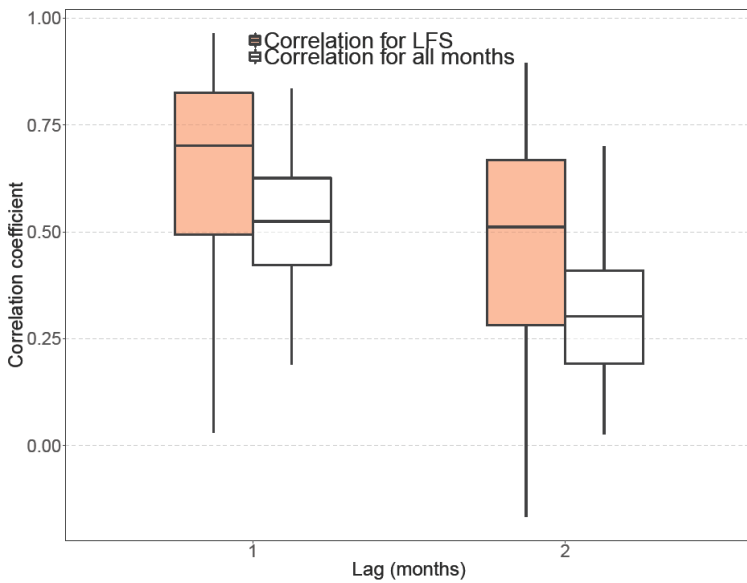
752 **Figure 1.** Updated Köppen-Geiger climatic map for period 1951–2000 (Kottek et al., 2006) showing the location of
 753 the 224 river gauge stations.



754
755
756
757
758

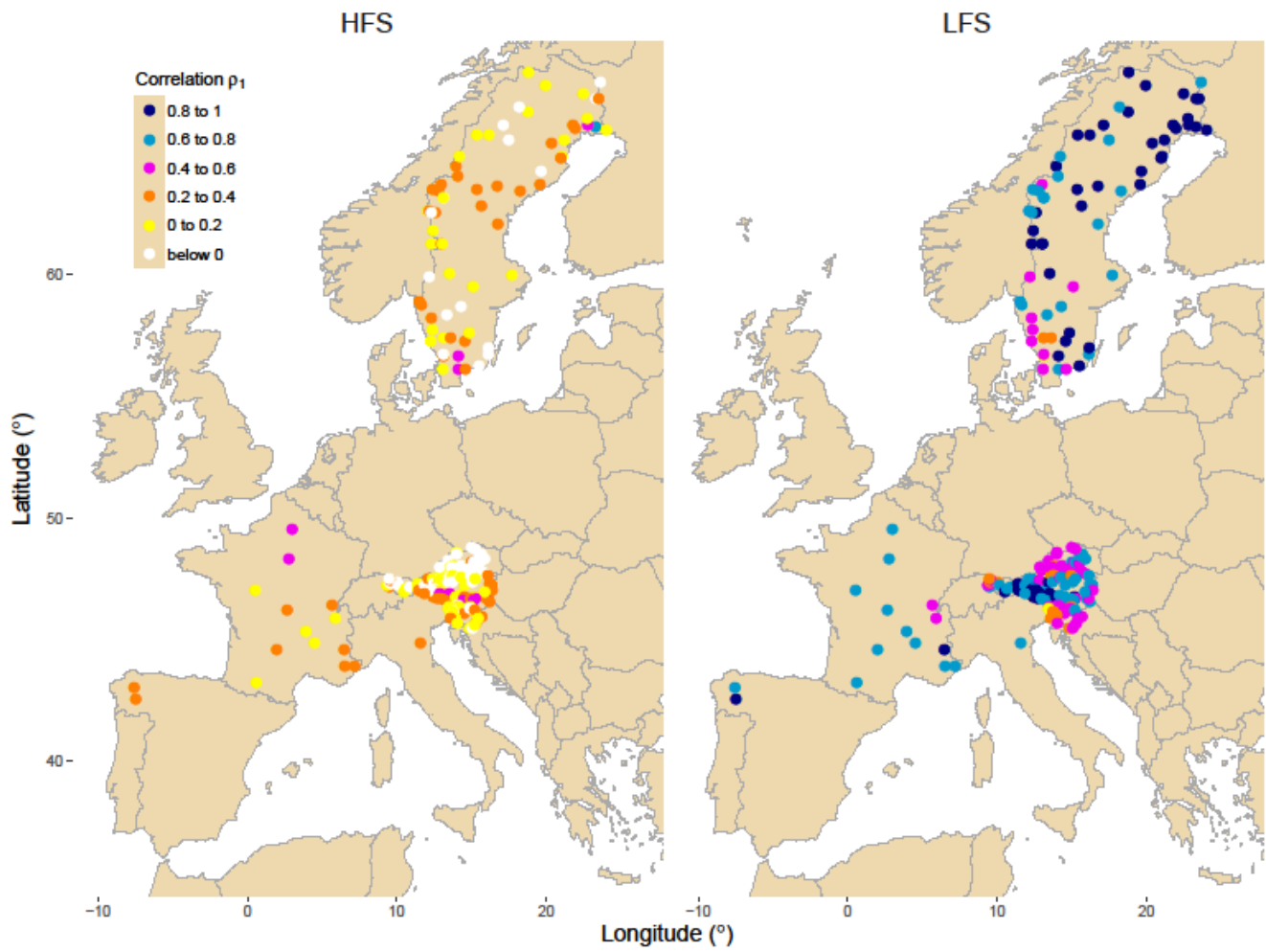
Figure 2. Boxplots of seasonal correlation coefficient against lag time for HFS (left panel) and LFS (right panel) analysis for the 224 rivers. The lower and upper ends of the box represent the 1st and 3rd quartiles, respectively, and the whiskers extend to the most extreme value within 1.5 IQR (interquartile range) from the box ends; outliers are plotted as filled circles.

759



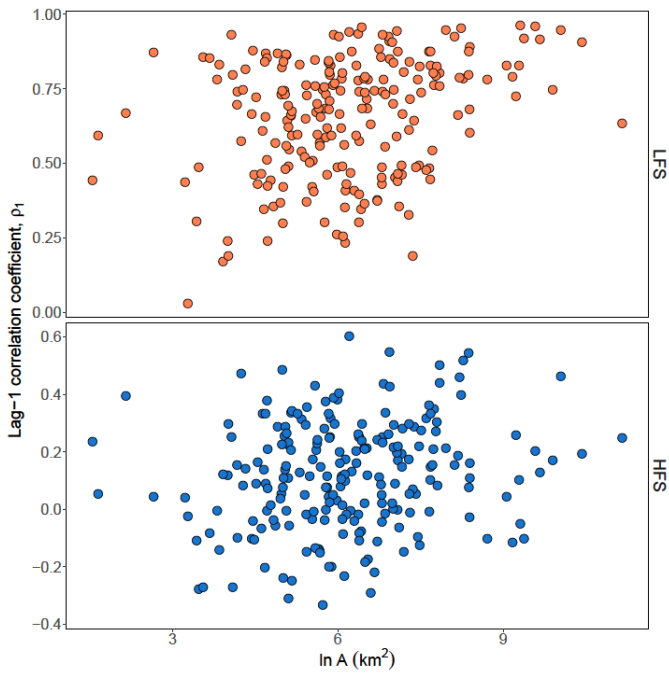
760
761
762
763

Figure 3. Boxplots of lag-1 and lag-2 correlation coefficients for LFS analysis (orange) and the whole monthly series (white) for the 224 rivers. The lower and upper ends of the box represent the 1st and 3rd quartiles, respectively, and the whiskers extend to the most extreme value within 1.5 IQR (interquartile range) from the box ends.



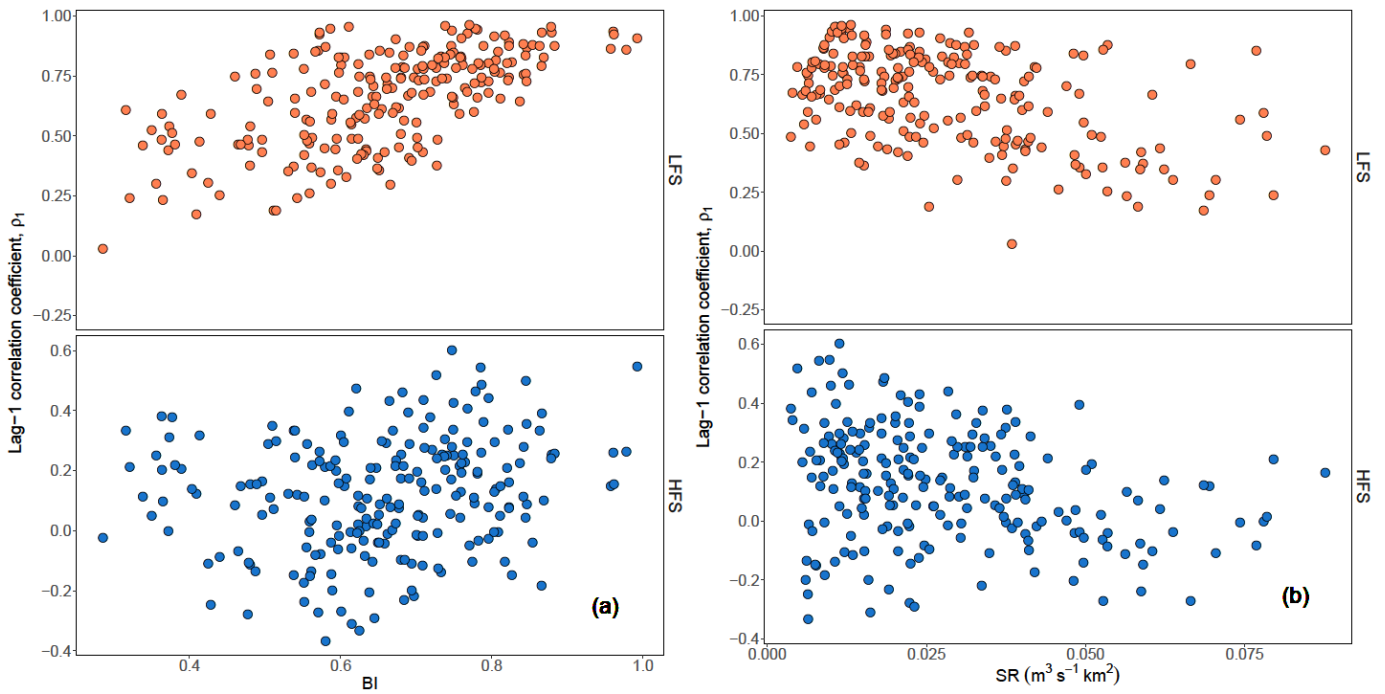
764 .

765 **Figure 4.** Spatial distribution of the lag-1 correlation coefficients for HFS (left) and LFS (right) analysis. Legend
 766 shows the color assigned to each class of correlation for the data.



767
768
769

Figure 5. Scatterplots of lag-1 HFS (bottom panel) and LFS (top) streamflow correlation versus the natural logarithm of basin area $\ln A$.



770

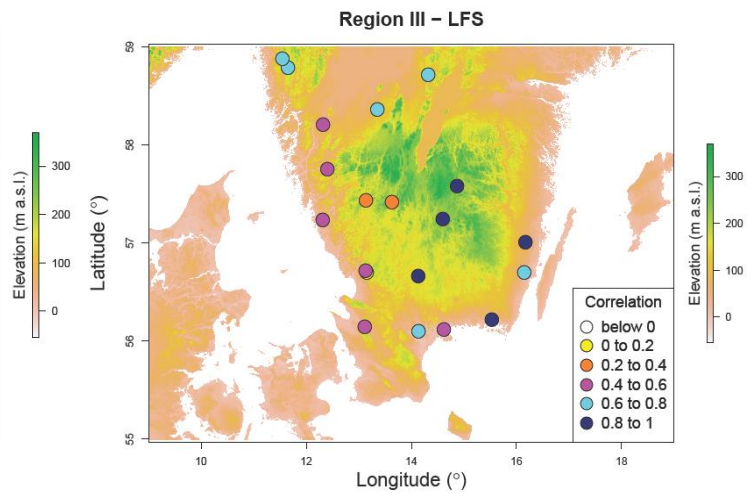
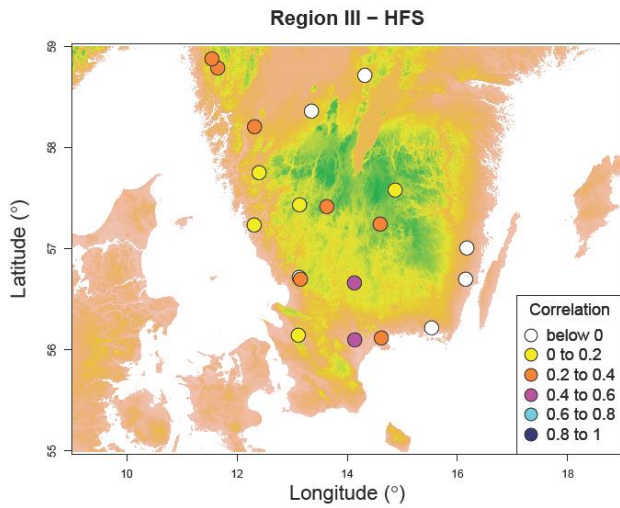
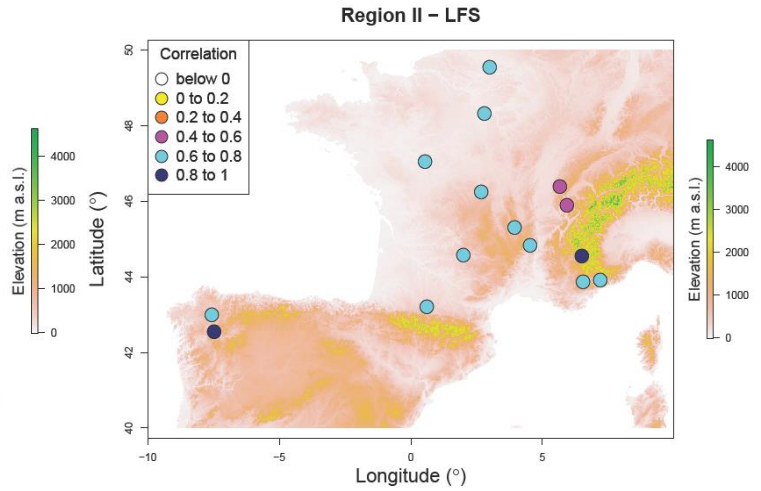
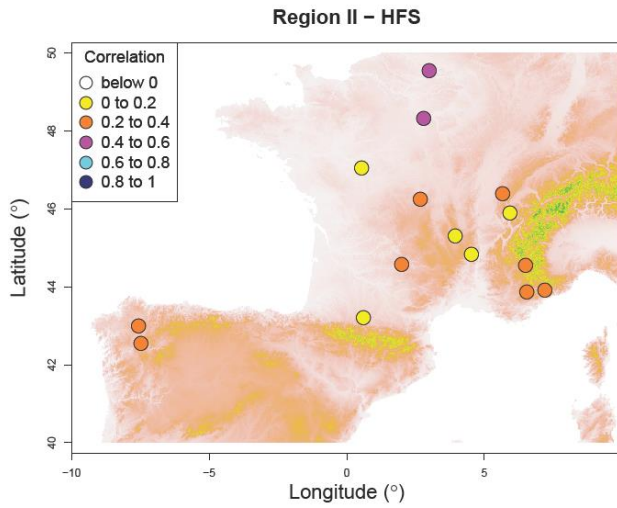
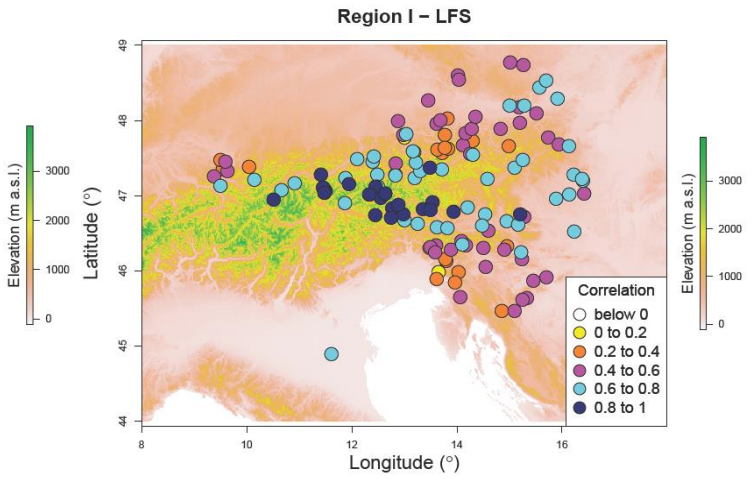
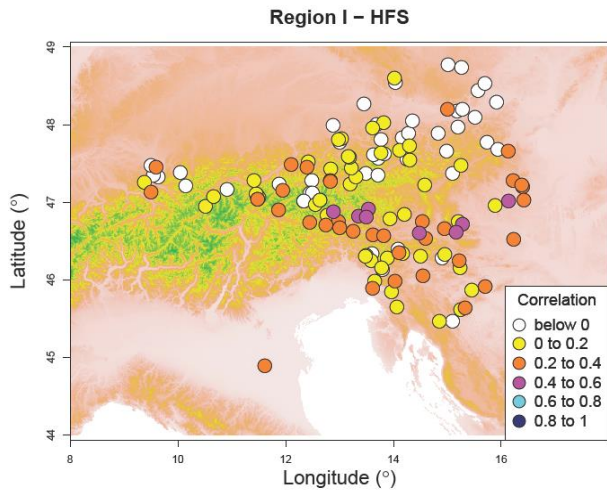
Figure 6. Scatterplots of lag-1 HFS (bottom panels) and LFS streamflow correlation (top panels) versus baseflow index BI (a) and specific runoff SR (b).

773

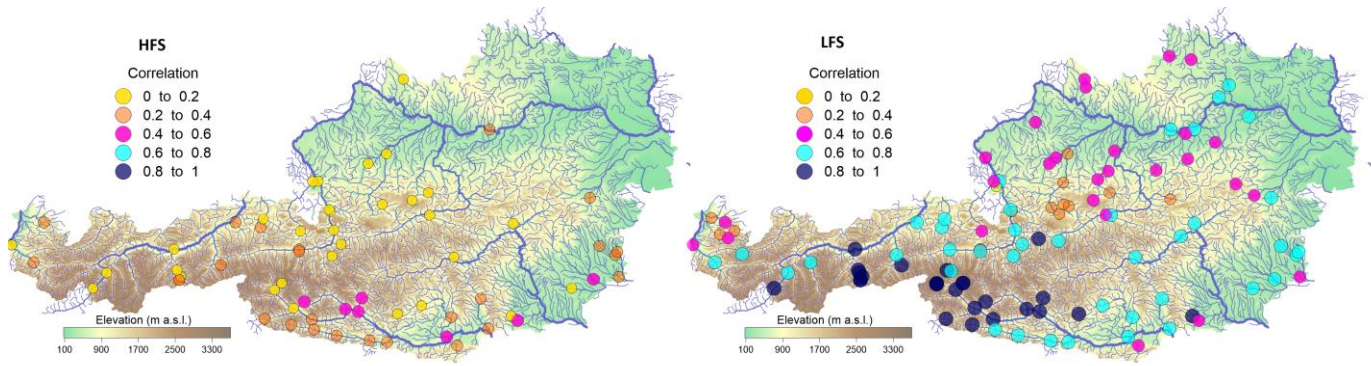
774

775

776

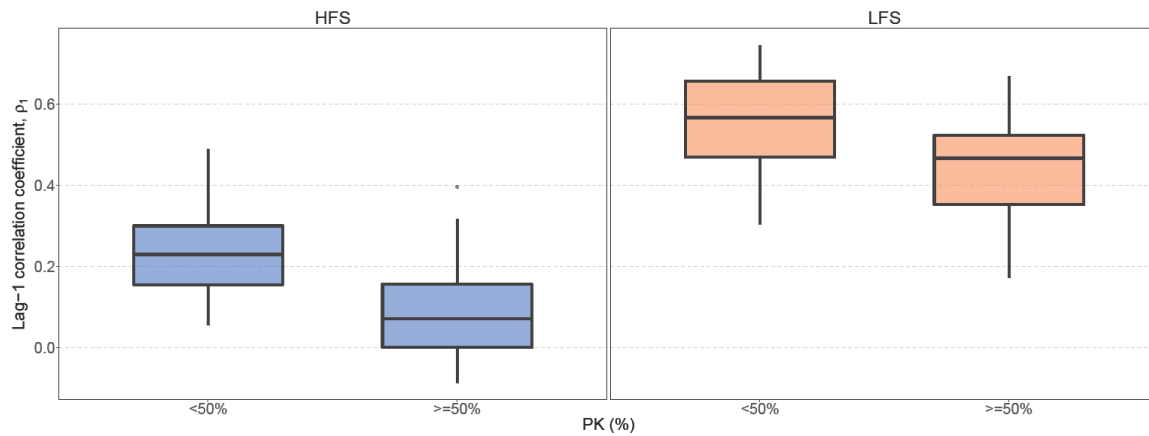


780 **Figure 7.** Relief maps from SRTM elevation data for the HFS and LFS lag-1 correlations of the rivers. Note that
 781 elevation scale is different for each region. Legend shows the colour assigned to each class of correlation for the data.



782
783
784
785

Figure 8. Digital elevation model of the Austrian river network depicting the spatial distribution of lag-1 positive correlation for HFS (left) and lag-1 positive correlation for LFS (right). Legend shows the colour assigned to each class of correlation for the data.

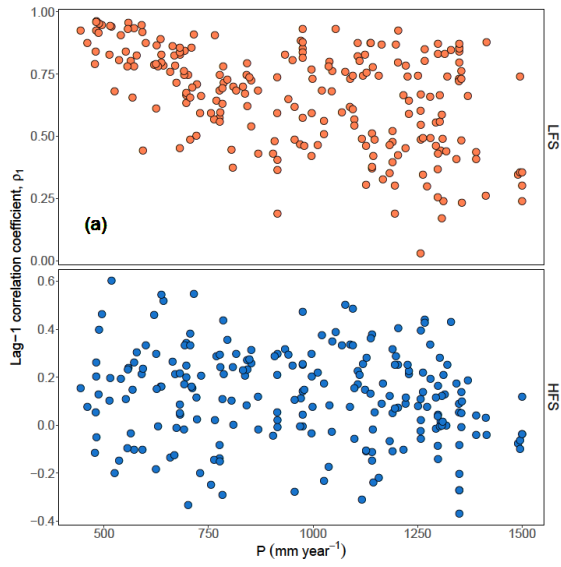


786
787
788
789
790

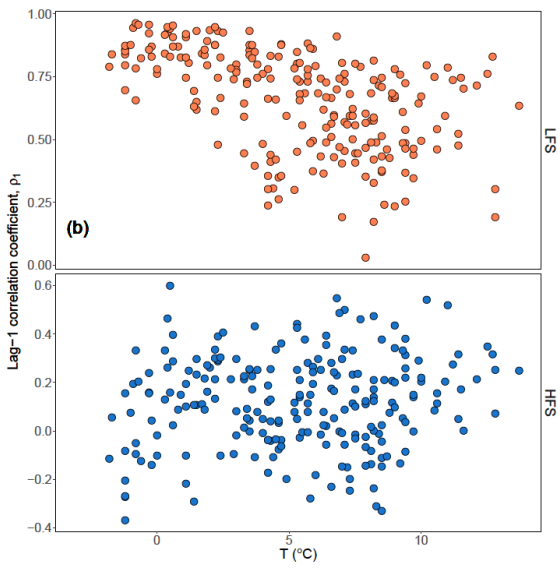
Figure 9. Boxplots of lag-1 correlation for Slovenian rivers with more than 50% presence of karstic formations PK and rivers with no or less presence for HFS analysis (left) and LFS analysis (right). The lower and upper ends of the box represent the 1st and 3rd quartiles, respectively, and the whiskers extend to the most extreme value within 1.5 IQR (interquartile range) from the box ends.

791
792
793
794
795
796
797

798



799



800

801

802

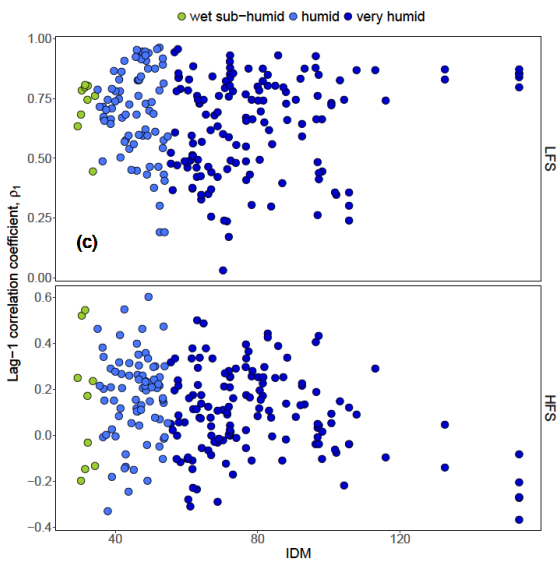
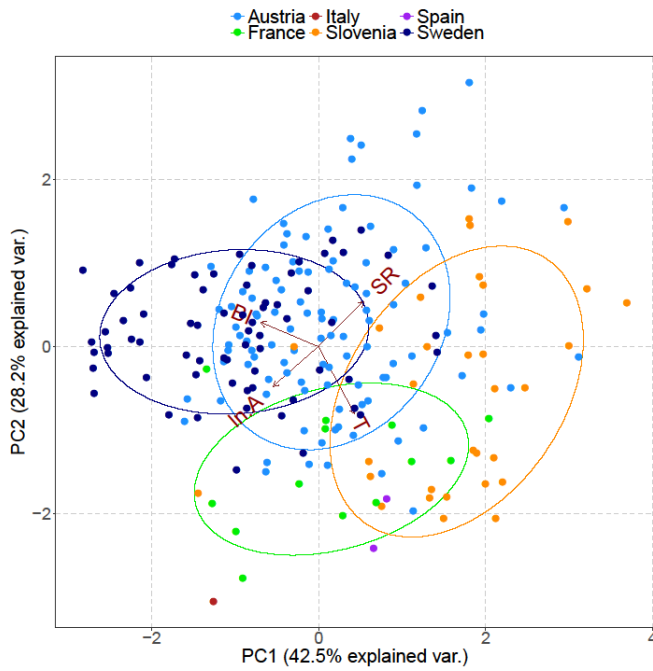
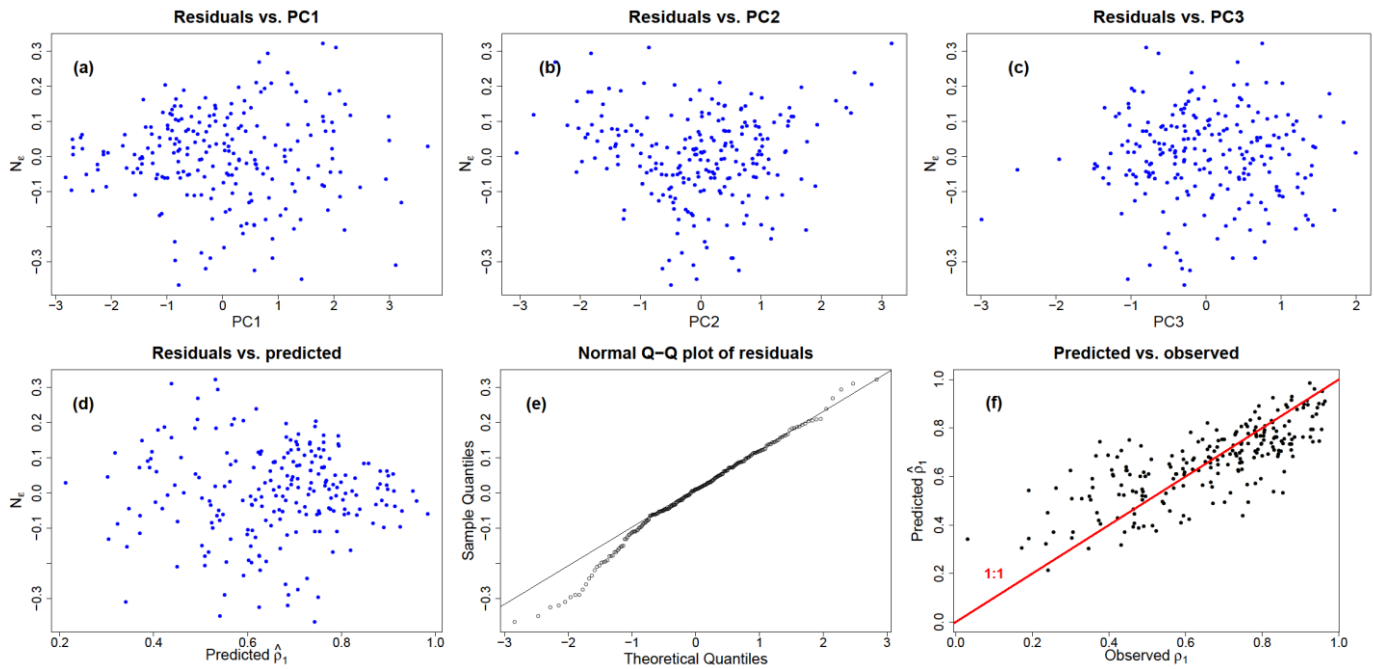


Figure 10. Scatterplots of lag-1 HFS and LFS correlation versus annual precipitation P (a), mean annual temperature T (b), and Index De Martonne IDM (c).



803

804 **Figure 11.** Principal component distance biplot showing the principal component scores on the first two principal
 805 axes along with the vectors (brown arrows) representing the coefficients of the baseflow index BI, specific runoff SR,
 806 natural logarithm of basin area $\ln A$ and mean annual temperature T variables when projected on the principal axes.
 807 Scores for the rivers are plotted in different colors corresponding to each country of origin and 68% normal
 808 probability contour plots are plotted for the countries.



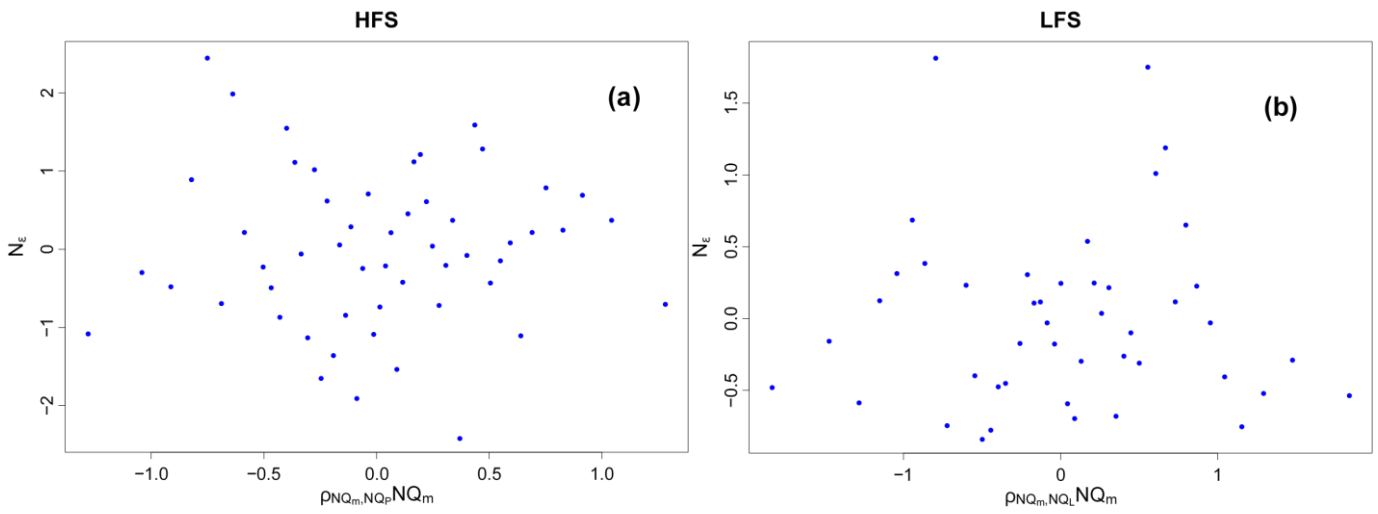
809

810

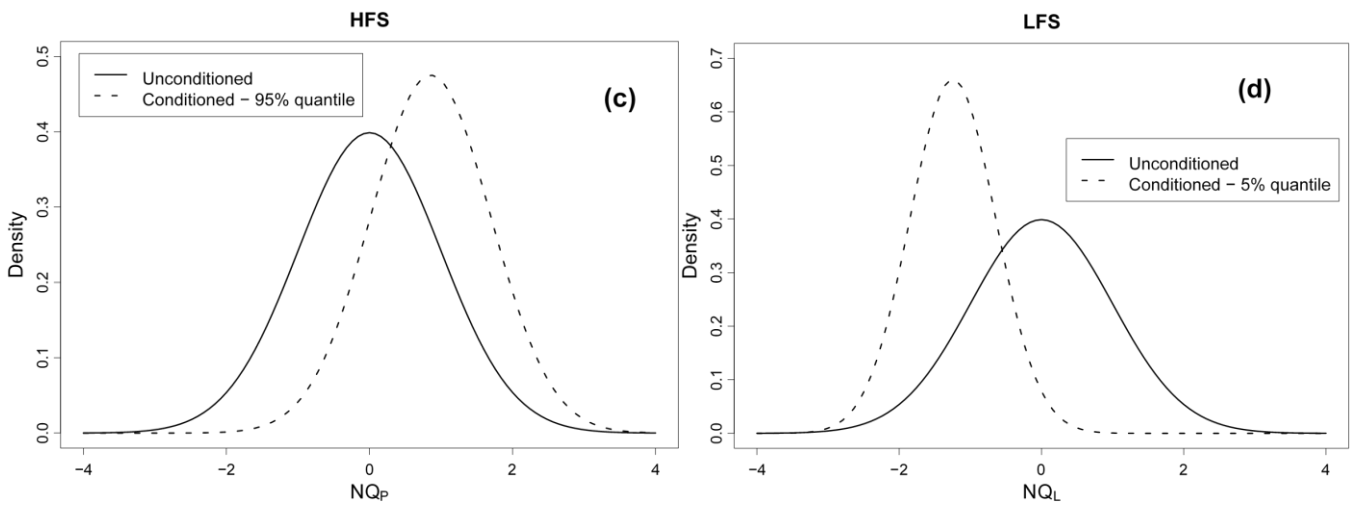
811 **Figure 12.** Diagnostic plots of linear regression for the LFS model. Residuals versus the first (a), the second (b) and
 812 the third principal component (c) and the predicted values (d). Normal Q-Q plot of the residuals (e). Plot of the
 813 predicted values from linear regression vs the observed ones; red line is the diagonal line 1:1 (f).

814

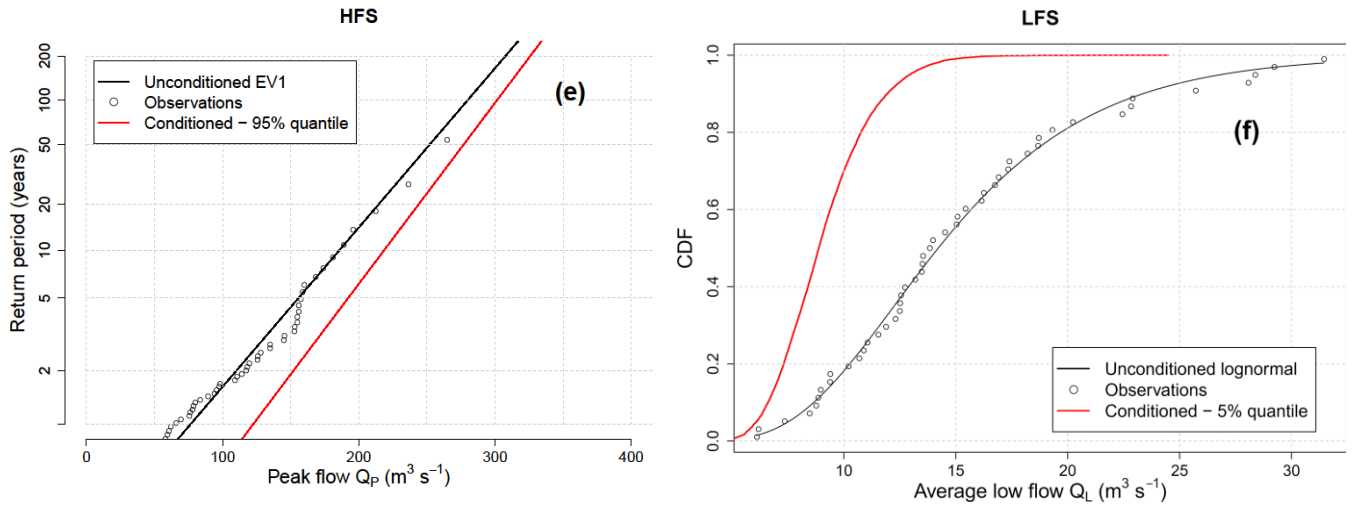
815



816



817



818

819 **Figure 13.** Conditioning the frequency distributions for high and low flows for the Oise River. Plots of the
820 residuals of the linear regression given by Eq. (2) for the HFS (a) and LFS (b) models. Probability
821 distribution of the unconditioned normalized peak flows NQ_P (solid line) and the normalized peak flows
822 NQ_P conditioned to the occurrence of the 95% quantile (dotted line) for the HFS (c) and probability
823 distribution of the unconditioned normalized low flows NQ_L (solid line) and the normalized low flows NQ_L
824 conditioned to the occurrence of the 5% quantile (dotted line) for the LFS (d). Gumbel probability plots of
825 the return period vs the unconditioned peak flows Q_P (black line) and the peak flows Q_P modelled by the
826 EV1 distribution and conditioned to the occurrence of the 95% quantile (red line) for the HFS (e) and
827 cumulative distribution function of the unconditioned low flows Q_L (black line) and the low flows Q_L
828 modelled by the lognormal distribution and conditioned to the occurrence of the 5% quantile (red line) for
829 the LFS (f).